Reactions and Single-Particle Structure of Nuclei Near the Drip Lines

P.G. Hansen and B.M. Sherrill*

National Superconducting Cyclotron Laboratory and
Department of Physics and Astronomy,
Michigan State University, East Lansing, Michigan 48824, USA.

The techniques that have allowed the study of reactions of nuclei situated at or near the neutron or proton drip line are described. Nuclei situated just inside the drip line have low nucleon separation energies and, at most, a few bound states. If the angular momentum in addition is small, large halo states are formed where the wave function of the valency nucleon extends far beyond the nuclear radius. We begin with examples of the properties of nuclear halos and of their study in radioactive-beam experiments. We then turn to the continuum states existing above the particle threshold and also discuss the possibility of exciting them from the halo states in processes that may be thought of as "collateral damage". Finally, we show that the experience from studies of halo states has pointed to knockout reactions as a new way to perform spectroscopic studies of more deeply bound non-halo states. Examples are given of measurements of l values and spectroscopic factors.

1. INTRODUCTION

The study of nuclei far from the valley of beta stability has progressed in a way that calls to mind the development of nuclear physics in its earlier days. Decisive insight into the structure of the nucleus came with the emergence of induced nuclear reactions as a tool. Rapid progress was made in the sixties with the development of accelerators and spectrometers allowing studies with high resolution. In a similar way, the challenging problem of studying the properties and structure of nuclei far from stability was clearly posed in 1966, the time of the first conference [1] in the series that currently is referred to as the ENAM conferences. However, for a long time to come and just as in classical nuclear physics, there were only two main methods available. One was based on studies of α, β and γ radiations from radioactive decays. The other involved measurements of ground-state properties: masses, spins, nuclear moments and charge radii (from optical isotope shifts). These techniques continue to play a role in modern studies of exotic nuclei, and number of examples can be found in the present volume [2].

A new era began only a little over a decade back, when reactions induced by radioactive beams entered the stage. The status of the field of exotic nuclei at this juncture in time has been documented in a volume edited by Bromley [3]. In this, an article by Tanihata [4] discusses the emergence of fast beams from fragmentation. The first application of

*This work was supported by NSF Grant No. PHY95-28844

this method [5] was to determine nuclear matter radii from measurements of interaction cross sections, a technique that continues to play an important role, see the review [6]. These pioneering experiments immediately gave a surprising result that drew attention to the new field. The cross sections for certain neutron-rich isotopes, ^{11,14}Be and ^{11}Li, turned out to be anomalously high. They were interpreted in terms of the formation of a nuclear halo, created by the penetration of the wave function of the last nucleon(s) to large distances, far beyond the central part of the nucleus. Soon after, this interpretation found confirmation in the observation [7] of a narrow transverse momentum distribution for the heavy residue in the breakup of a halo system. Qualitatively, this is what should be expected from Heisenberg's uncertainty principle. The extended wave function in spatial coordinates is represented by a narrow wave function in momentum coordinates. In the following years a large effort has been dedicated to the study of halo systems. Recently, it has become clear that some of the techniques developed for the halo have a wider applicability to non-halo states.

This review is divided into three main parts. We begin by a discussion of some of the salient features of halos and their reactions. The next section deals with single-particle structure in neutron-rich ensembles that have no bound states (i.e. that are "beyond the drip lines"), and it gives an overview of other continuum and threshold effects in experiments. The last section discusses the extension of direct-reaction methods, first developed for halos, to non-halo states. It will be shown that it is possible to perform precision spectroscopy via single-nucleon knockout reactions in inverse kinematics at typically 50-1000 MeV/nucleon. In these experiments, the shapes of the parallel-momentum distributions of the projectile residues determine the l values while the absolute cross sections to specific final levels give spectroscopic factors.

2. STRUCTURE AND REACTIONS OF HALO NUCLEI

For many nuclei close to the drip lines, the weak binding of the last nucleon (or nucleon pair) may lead to a wave function with an external "tail" extending far outside of the nuclear core as a result of quantum mechanical barrier penetration. This structure is referred to as a halo state, see the reviews [8–10] and a number of papers in [11]. Examples of single-neutron halos are the ground states of ^{11}Be, ^{14}B, ^{15}C, and ^{19}C. Since the binding energy of a halo neutron is small as well as critical for its properties, it has become customary to calculate the radial wave functions in a potential-well model that reproduces the experimental separation energy. It is usually necessary to evaluate radial integrals out to very large distances (40-100 fm). Halos with two neutrons depend on the n-n interaction for their stability. The best cases, so far, are ^{6}He, ^{11}Li, and ^{14}Be.

Proton halos are less pronounced because of the Coulomb barrier. This is the general reason why the shell models based on effective interactions work well in describing the properties of proton-rich nuclei. There are, however, cases where the extended wave function of a proton halo becomes important. The (weak) tail of the l=1 odd proton orbital of ^{8}B is well known for its role in the solar neutrino problem, and the l=0 excited level at 495 keV in ^{17}F is also of considerable interest to nuclear astrophysics [12]. For the ^{8}B case, Mukhamedzhanov and Timofeyuk [13] and also Esbensen and Bertsch [14] have discussed how it is necessary to introduce wave functions with the correct asymptotic

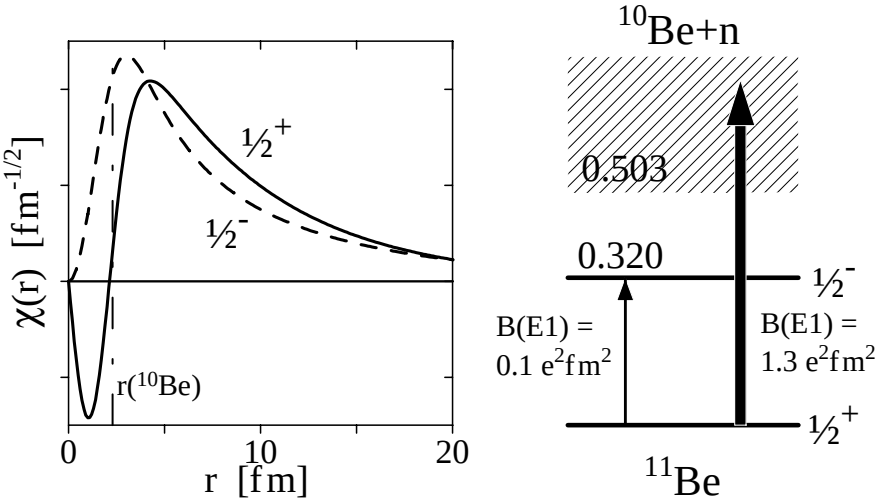

Figure 1. Radial wave functions $\chi(r) = rR(r)$ for the single-particle components of the $1s_{1/2}$ and $0p_{1/2}$ levels in ^{11}Be, bound by 0.503 and 0.183 MeV, respectively. Their rms radii are 7.26 and 6.31 fm, respectively. The radius of the ^{10}Be core of 2.36 fm is indicated by the dotted-dashed line. The level scheme shows the measured reduced E1 transition probabilities (in e^2fm^2) between the states and from the ground state to the continuum.

behavior in order to describe reactions at large distances. The former paper makes use of the exact analytical form of the Coulomb wave function and the latter of a Woods-Saxon wave function. Proton halos with l=0 are not encountered as ground states until the light phosphorus isotopes [15], where the $1s_{1/2}$ state fills following the Z=14 sub-shell closure. Here the Coulomb barrier is already so high that the tails of the halo wave functions are not very pronounced, as can be seen from a figure in this paper. This assignment has been confirmed experimentally [16].

An effect similar to the halo arises from the large difference in the Fermi energies for protons and neutrons in nuclei with a large neutron excess. This results in a neutron radius that is markedly larger than the proton radius, a phenomenon that has been named the "neutron skin" [17]. An example of this is ^{8}He, which also may be thought of as a four-neutron halo. The actual size of the skin is also related to the symmetry energy between neutrons and protons [18]. On theoretical grounds the skin is believed [19] to lead to a more diffuse nuclear surface, which has interesting consequences for the spin-orbit interaction and for the pairing in nuclei close to the drip lines. For the sodium isotopes, experimental information is available on both the proton and neutron radii, and this has been compared with microscopic calculations based on density-dependent Skyrme interactions [20]. The Skyrme method can relate properties of exotic nuclei over a wide mass range [18], and it has been used by Brown [21] to give an important new constraint on the equation of state for neutron matter.

Many papers have discussed the structure and reactions of halo states and a general review is not possible within the constraints of the present paper. We use in the following sub-sections the example of the nucleus ^{11}Be to illustrate some of the main features. The radial wave functions corresponding to the (dominant) single-particle components of its

two (only) bound states are shown in Fig. 1. The $\frac{1}{2}^+$ and $\frac{1}{2}^-$ states are both halos; they have 91% and 87%, respectively, of the probability outside of the ^{10}Be *rms* radius of 2.36 fm.

2.1. Basic Properties of Halo States

Excellent overviews of the properties of halo nuclei have been prepared by Riisager, Fedorov and Jensen [9], and by Jonson and Riisager [10]. The basic conditions for the occurrence of one- and two-neutron halo systems have been discussed in Refs. [22,23]. Halos are found in systems bound by short-range interactions and require that the ground-state wave function has an appreciable single-particle component. Furthermore, pronounced halos are only possible for low values of the angular momentum. Two-body halos with l=0 or 1 have a diverging *rms* radius as the binding approaches zero. If three-body halos are described in an expansion in hyperspherical harmonics, see Zhukov *et al.* [24], the appropriate quantum number is the hypermomentum K. For halos with a neutron pair in a 0^+ state, the favored values of K are 0 or 2. Because of the Coulomb barrier, a proton halo will remain finite [22], even as the separation energy approaches zero.

A recent paper has considered for which nuclei one has the best chance of encountering halo systems [25]. Basically these are the regions where l=0,1 states appear at the Fermi surface. It is possible, however, that changes in the nuclear surface due to weak binding and skins may change the level order and lead to low l states in many drip-line nuclei. Mizutori *et al.* [26] have looked at the possibility of halo and skin systems in heavier nuclei using mean field calculations. They find that pairing may be a dominating effect and could limit the number of halo cases. A similar conclusion was reached by Bennaceur *et al.* [27], who find a possibility of large halos in odd-N nuclei but a "pairing anti-halo effect" in even-N nuclei. (The existence and nature of strong pairing is, of course, also of interest in itself.) Finally, an interesting possibility in two-nucleon halo systems is the existence of Efimov states. These states, which would be bound by only a few keV, are a three body effect in which the valence neutrons can extend to a size of 100 fm or more [28]. At present there is no experimental evidence for such states, but the problem continues to draw theoretical interest, see [29,30].

It is interesting that halos, so far, only have been directly observed in nuclear physics experiments, although other areas of quantum physics offer systems with the right properties. The paper of Riisager *et al.* [9] uses a scaling relationship to relate sizes and binding energies of two-body halo systems taken from different areas of quantum physics. Theoretical estimates point to systems that could have considerably larger radii in these units than the nuclear halos. In molecular physics, an example would be the helium dimer, bound by the van der Waals force. In particle physics, the only example seems to be the hypertriton consisting of a Λ orbiting a deuteron. Halos are not possible in neutral atoms, for which an electron always must experience the long-range Coulomb potential at large distances. The Rydberg states, in spite of their large size, are not halos but natural members of the Balmer series. On the other hand, negative ions, which have vanishing interaction at large distances between an electron and the neutral residue, can become very large. A special case is the binding of an electron to a molecule with a very large electric dipole moment, a general phenomenon predicted by Fermi and Teller [31]. The effect has recently been observed in some cases. For the acetonitrile molecule, studied by

Desfrancois *et al.* [32], the dipole bound state is actually the ground state of the negative ion since acetonitrile has negative electron affinity. If the electron attaches itself to the core, as is the case for the negative hydrogen ion, the electronic halo is small [9].

It is characteristic of weakly bound nuclei that their continuum structure plays a much more prominent role than it does for normal nuclei. A typical halo nucleus has only a few bound states and often only one, and couplings to single-particle unbound states may give appreciable strength at low energy. In connection with the electric excitation of the ^{11}Li halo, this was referred to [33] as a "very soft" dipole mode in the meaning of a low-frequency single-particle excitation. In heavier nuclei, the coupling of low-lying resonance modes to the giant resonance(s) may be more complex and have a more collective character. For example, Hamamoto *et al.* [34] have investigated the resonance structure of drip line nuclei using QRPA and found that considerable isovector and isoscalar dipole strength is moved to lower excitation energies. We shall return to these problems in connection with the discussion of electric properties of halo systems. Theoretical calculations of halo systems can become quite complex. It is imperative to allow for the large size of wave functions, and often strong non-perturbative couplings to intermediate states (and the continuum) and final-state interactions from resonances [35,36] have to be included. Such strong effects have been seen experimentally, for example, in the Coulomb excitation of ^{8}B near the barrier energy [37].

Studies of beta and gamma decays and of beta-delayed particles have played an important role in halo studies. The original discovery of the neutron halo by Millener *et al.* [38] came as a conclusion based on the surprisingly short lifetime of the $\frac{1}{2}^-$ excited state of ^{11}Be, see Fig. 1. The emission of deuterons and tritons following beta decay, discussed in the review by Jonson and Riisager [39], is linked directly to the low binding of the halo neutrons. In a recent experiment on the beta decay of ^{11}Li, Borge *et al.* [40], see also ref. [39], obtained beta-decay matrix elements from measurements of beta-delayed neutrons. They used this to confirm the theoretical expectation that the last neutron pair is in a strongly correlated state with a fifty-fifty mix of the regular p^2 component and an s^2 intruder. Other experiments that support this finding will be discussed below. The main tool in halo studies has, however, been nuclear reactions observed with the halo state as the beam particle in what is usually referred to as inverse kinematics. We devote the following subsections to this aspect and in particular to one-nucleon removal reactions, which have become a very valuable tool for elucidating halo structure.

2.2. Electromagnetic Excitation of Halo States

The transition probability between the bound states of ^{11}Be has been re-measured in intermediate-energy Coulomb excitation experiments in inverse kinematics, see Ref. [41] and references therein. These confirm that the reduced transition probability B(E1) indeed is as large as 0.1 e^{2}fm^2. By normal standards, this is a very large value for a transition between low-lying bound states. Still, it is more than an order of magnitude smaller than that of the E1 transitions of low energy leading from the ground state to the ^{10}Be+n continuum, see Fig. 1. The large magnitude of the dissociation cross sections in intermediate-energy collisions of halo states with high-Z nuclei offers strong evidence for the halo, see Fig. 2 based on data and calculations from [42–45], and corroborates information from interaction cross sections [17] and momentum distributions [46]. (Here

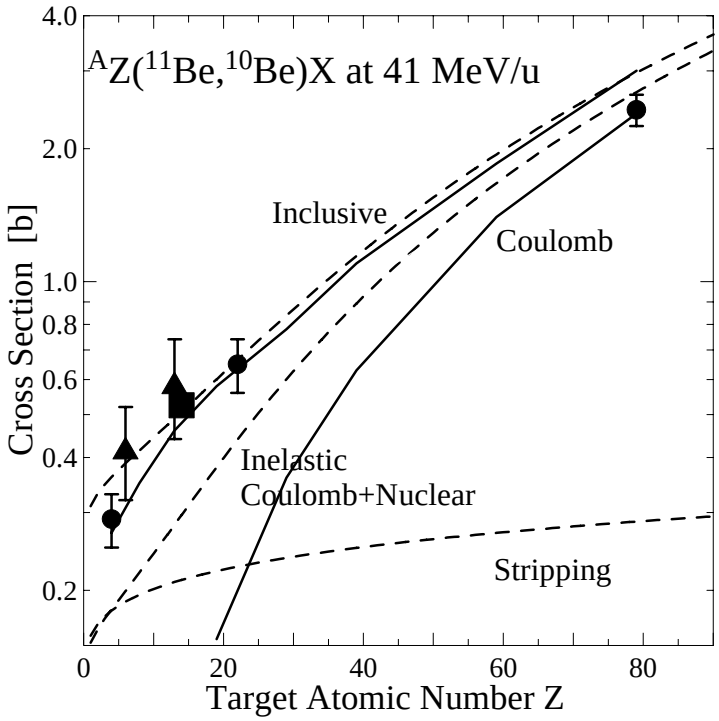

Figure 2. Measured inclusive cross sections for the (^{11}Be,^{10}Be) reaction at 41 MeV/nucleon on targets of Be, Ti, Au (circles) [43] and Si (square) [44]. Data at 33 Mev/nucleon on C and Al [42] (triangles) have been downscaled by 10% to compensate for the energy difference. The full-drawn lines are the calculations by Hencken *et al.* [45] of the Coulomb and inclusive removal cross section. The dashed lines represent a schematic calculation [43] based on a simplified black disc model but including Coulomb-nuclear interference. The calculations assume a $1s_{1/2}$ spectroscopic factor of unity, whereas the currently accepted values [46] are 0.74 ($1s_{1/2}$) and 0.18 ($0d_{5/2}$). Inclusion of these would improve the agreement with the measured inclusive cross sections.

and in the following, we refer to reactions of the type (^{11}Be,^{10}Be) as dissociation reactions, whether or not the removed neutron is observed.)

The general theory of Coulomb dissociation reactions of halo nuclei has been discussed by a number of authors, see [47–51]. The striking feature is that the absolute E1 cross sections can be accounted for almost quantitatively by a model in which both the ground state and the continuum final states are taken to be extreme single-particle states. Since all possible excitation channels of the core-nucleon system are included in this picture, it follows that the low-energy spectrum exhausts the appropriate "molecular" sum rules given by Alhassid *et al.* [52]. In their simplest form, corresponding to a single neutron coupled to an inert nuclear core, they have frequently been applied to halo systems [33,53–55]. The approximate non-energy-weighted and energy-weighted sum rules, expressed in terms of the final kinetic energy E, are

$$\Sigma_0 = \int_{-\infty}^{\infty} dE \frac{dB(E1)}{dE} = \frac{3}{4\pi}\left(\frac{Ze}{A}\right)^2 \langle r^2 \rangle \qquad (1)$$

and

$$\Sigma_1 = \int_{-\infty}^{\infty} dE \frac{dB(E1)}{dE}(E - E_{gs}) = \frac{9}{4\pi}\left(\frac{Ze}{A}\right)^2 \frac{\hbar^2}{2\mu}, \tag{2}$$

where μ is the reduced mass. Eq. (1) has been verified directly by Nakamura *et al.* [56], who found Σ_0 to be 1.3 ± 0.3 e^{2}fm^2. With an assumed *rms* halo radius of 7.26 fm taken from Fig. 1 one obtains a theoretical value of 1.66 e^{2}fm^2 from Eq. (1), which reduces to 1.23 if it is taken into account that the spectroscopic factor of the halo configuration must be close to 0.74, see Ref. [46].

The observation of the energy spectrum [56] (discussed again in section 3) and the absolute differential cross section as a function of angle [43] prove the validity of the energy-weighted sum rule. The ratio of the two sum rules gives the average excitation energy

$$\langle E^* \rangle = \frac{3\hbar^2}{2\mu\langle r^2\rangle} \approx \frac{6S_n}{1+x}, \tag{3}$$

where the last expression assumes a bound l=0 state with the neutron separation energy S_n, and x is a finite-size correction of order unity. One finds $\langle E* \rangle$=1.5 MeV for Coulomb excitation of ^{10}Be+n. The prevalence of strength at low energy is also observed for two-neutron halos, and the sum rule has been used [33] to give a rough prediction of 0.9 MeV for the average ^{11}Li excitation energy in Coulomb excitation in good agreement with experiment [57]. The strong E1 transitions to the continuum are, of course, also felt strongly in the inverse channel corresponding to direct neutron capture. This was discussed very early by Uchiyama and Morinaga [58] and later in papers by Mengoni *et al.* [59].

According to Eq. (3) the average $E1$ excitation energy is inversely proportional to the square of the halo radius and roughly proportional to the separation energy of the halo neutron. The intense continuum strength just above the particle threshold becomes, so to say, a mirror image of the bound state existing just below threshold. We return to the phenomenon of threshold effects in section 3. The large E1 strength at low energies contrasts in a dramatic way with the properties of "normal" nuclei (the deuteron excepted) and is reminiscent of the photoelectric process in an atom, which also has essentially single-particle strength. For nuclei near the valley of beta stability, the coupling to the giant dipole resonance typically reduces the electric dipole strength of low-energy E1 transitions by several orders of magnitude. It is interesting that this strong hindrance is relaxed also in some more stable nuclei, for which cluster structures are believed to play a role. The work by Gai *et al.* [60–62] found cases where the E1 transition strength reached approximately one hundredth of a Weisskopf unit, still weak compared with the halo systems,

The Coulomb method has been applied to many cases. As an illustration of its power we can take the Coulomb breakup of ^{19}C. For this isotope, Nakamura et al. [63] have recently shown from their Coulomb dissociation data that the ground state is $\frac{1}{2}^+$ and that the binding energy is in the range of 600 keV, considerably larger than suggested by other experiments. This makes ^{19}C a well-developed single-neutron halo system, comparable to ^{11}Be.

2.3. Nuclear Reactions of Halo States

This Section deals principally with the dissociation of halo states via nuclear interactions. Still, we would like initially to remind the reader of other types of reactions that also have contributed to the understanding of nuclear halos.

2.3.1. Total, elastic and fusion cross sections

As mentioned in Sect. 1, the measurements of interaction cross sections have been of primary importance as a source of information about matter radii, see the recent papers refs. [6,64]. Elastic and inelastic scattering experiments have been made for halo and skin nuclei by using inverse kinematics, where the role of target and beam are interchanged. For example, proton elastic scattering of ^{11}Li has been studied at GSI and RIKEN by bombarding hydrogen targets by a ^{11}Li beam [65–67] and compared with theoretical models, see *e.g.* Ref. [68].

An interesting question is the effect the halo will have on fusion-evaporation reactions near barrier energies. One might imagine that the halo could significantly enhance these cross sections. On the other hand, the weak binding of these nuclei could lead to breakup effects that diminish the cross sections. Attempts have been made by various authors to measure and understand these effects. The transfer and breakup modes of ^{6}He on ^{209}Bi were studied recently with the radioactive beam facility at Notre Dame University [69]. The result was a large neutron transfer cross section, which may account for the large observed sub-barrier fusion enhancement in this system [70]. A more recent experiment performed at the Louvain-la-Neuve radioactive beam facility has also seen evidence for fusion enhancement at near and below barrier energies in a comparison of ^{4}He and ^{6}He induced fusion [71]. Various experiments have searched for enhancement in fusion cross sections due to the halo. Experiments at RIKEN [72] and GANIL [73] have used a ^{11}Be beam to search for such an enhancement. A radioactive ^{17}F beam was used at Argonne National Laboratory to search for the effect in a proton halo case [74].

2.3.2. Dissociation of the single-neutron halo

The cross sections for Coulomb dissociation of halo nuclei are remarkably large, up to several barns. However, reactions with light targets also show large cross sections and narrow momentum distributions. The first such case was the observation [7] of a narrow transverse momentum distribution of ^{9}Li fragments from the reaction of ^{11}Li on a carbon target. General reviews of the reaction mechanisms within the framework of simple nuclear models have been given by Barranco and Vigezzi [75] and by Jonson [76].

Nuclear reactions at intermediate and high energies may conveniently be treated in the eikonal approximation, which is valid if the energy is high and the scattering angle small. The form known as Glauber theory has been widely used for calculating nucleon-nucleus and nucleus-nucleus reactions at high energies. At the same time the collision time is short, so that it becomes permissible to treat the evolution of the final states in the sudden approximation. The paper by Bertsch, Brown and Sagawa [77] and subsequent work [78,79,45] has applied these techniques to halo interactions with light targets. From the eikonal model it also follows that the outgoing fragment's longitudinal momentum distribution reflects the momentum content of the wave function in the volume sampled by the projectile's interaction with the target [80–82]. The cross sections and momentum distributions are thus very sensitive to the angular momentum and separation energy of

the nucleon in the initial state.

In this article we will use the notation of Tostevin [83]. It is assumed that the nucleon is described by a normalized single-particle wave function with quantum numbers (nlj) moving with respect to the core of remaining nucleons in state $c \equiv I^\pi$. Such configurations are written $|\phi^c_{JM}\rangle$, where J is the magnitude and M the projection of the projectile's ground-state total angular momentum, $\vec{J} = \vec{I} + \vec{j}$. In the most frequent type of experiment, in which only the heavy residue is detected and not the neutrons, the single-particle cross sections are a sum of two contributions. These are usually referred to as elastic breakup (diffraction dissociation) and absorption (stripping) [84], so that we have $\sigma_{sp} = \sigma^{diff}_{sp} + \sigma^{str}_{sp}$. In the former, the nucleon and the heavy residue emerge from the reaction with essentially beam velocity. In the latter, the nucleon is scattered inelastically. These two contributions are computed separately, as integrals over the projectile's center of mass impact parameter, using [83]

$$\sigma^{diff}_{sp} = \frac{1}{2J+1} \int d\vec{b} \left[\sum_M \langle \phi^c_{JM}| \, |(1 - \mathcal{S}_{\rm c}\mathcal{S}_{\rm n})|^2 |\phi^c_{JM}\rangle - \sum_{M,M'} |\langle \phi^c_{JM'}|(1 - \mathcal{S}_{\rm c}\mathcal{S}_{\rm n})|\phi^c_{JM}\rangle|^2 \right] \quad (4)$$

and

$$\sigma^{str}_{sp} = \frac{1}{2J+1} \int d\vec{b} \sum_M \langle \phi^c_{JM}|(1 - |\mathcal{S}_{\rm n}|^2)|\mathcal{S}_{\rm c}|^2|\phi^c_{JM}\rangle. \quad (5)$$

Here the quantities $\mathcal{S}_{\rm c}$ and $\mathcal{S}_{\rm n}$ are the elastic S-matrices, or profile functions [85,86], for the core-target and removed neutron-target systems, expressed as functions of their individual impact parameters. These are calculated using the optical limit of Glauber theory [87]. The neutron-core relative motion wave functions $|\phi^c_{JM}\rangle$ are usually calculated in a Woods-Saxon potential with the depth of the potential adjusted to reproduce the separation energy of the nucleon. For high energies, for high l values, and for deeply bound states, the contribution from Eq. (5) is the largest, typically by a factor 2-3.

Equation (5) allows a simple interpretation. It is the integral over impact parameter and average over M substates of the joint probability of the core being left intact by the reaction (given by the quantity $|\mathcal{S}_{\rm c}|^2$) and of the nucleon being absorbed (given by the quantity $(1 - |\mathcal{S}_{\rm n}|^2)$). The diffractive cross section, Eq. (4), is derived within the spectator core plus nucleon model by using closure to eliminate the necessary integral over all continuum final states of the dissociated core and nucleon. The use of closure for obtaining the continuum contribution is clearly an excellent approximation for halos, where the ground state often is the only bound state. It is more doubtful how well it applies to deeply bound states such as the applications to be discussed in Sect. 4. Fig. 2 compares the results obtained for the removal cross sections ^{11}Be in two eikonal models, one very simple and one more realistic.

Theoretical calculations of the longitudinal momentum distributions of the core fragments may without significant loss of accuracy be made in a simpler model, based on the black-disc approximation [81,82]. In this, $\mathcal{S}_{\rm c}$ and $\mathcal{S}_{\rm n}$ are assumed to be unity outside of a cutoff impact parameter and zero inside [81]. A good choice for core impact parameter cutoffs is to define them to reproduce core-target reaction cross sections [88], respectively the free-neutron reaction cross section (approximately 290 mb on a beryllium target at

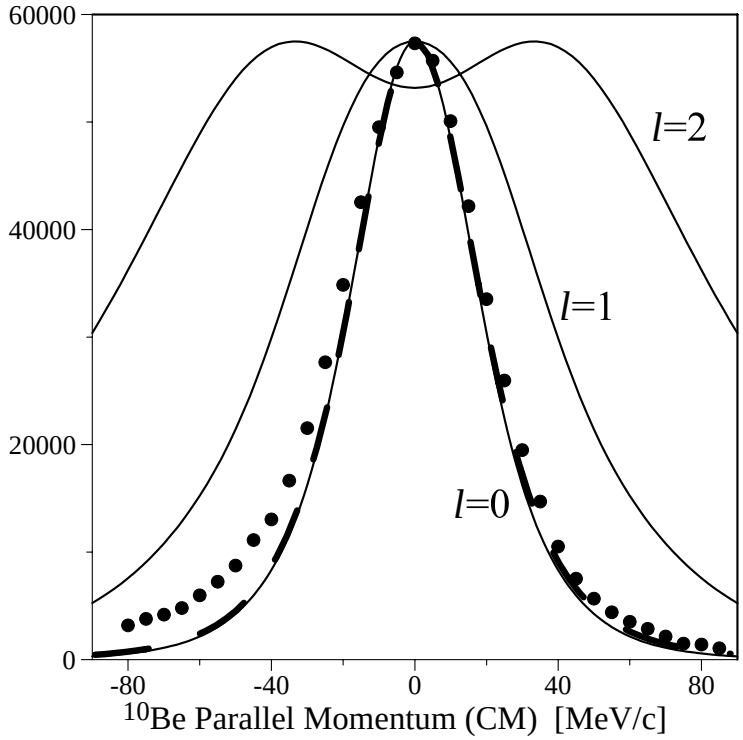

Figure 3. The experimental longitudinal momentum distribution [46] for the ^{9}Be(^{11}Be,^{10}Be$_{gs}$)X reaction at an incident energy of 60 MeV/nucleon. The experimental data have been corrected for a 22% contribution from reactions leading to ^{10}Be excited levels. The errors are smaller than the point size. The full-drawn lines are calculations for l=0,1,2 in an eikonal approximation [46] and the heavy dashed line is the time-dependent treatment by Bonaccorso and Brink [91]. The calculations have been adjusted to the maximum height of the data (in arbitrary units).

60 MeV/nucleon). The widths of the momentum distributions are quite insensitive to the precise choice of the target radius and even the absolute cross sections agree well with more accurate approximations. As an example, Fig. 3 from the work of Aumann *et al.* [46] shows the longitudinal momentum distributions from the ^{9}Be(^{11}Be,^{10}Be$_{gs}$)X reaction. As we know today, the original experiment [89] that found the narrow distribution on a light target included a 22% contribution of reactions leading to excited states. This has been subtracted in the data of Fig. 3, which shows good agreement with the calculation assuming l=0 and definitely excludes l=1,2. There are small but distinct deviations, a slightly larger width and also an excess of events (a "tail") on the low-momentum side. It has recently been demonstrated by Tostevin that these effects arise in the diffractive channel. They are linked to energy conservation and can be accounted for in a fully quantum-mechanical calculation based on the discretised continuum coupled-channels method [90].

An alternative treatment, by Bonaccorso and Brink, has also been applied to the longitudinal momentum distributions of neutrons from the breakup of halo states [91–93]. They use a semi-classical (constant velocity, straight line) approximation for the relative

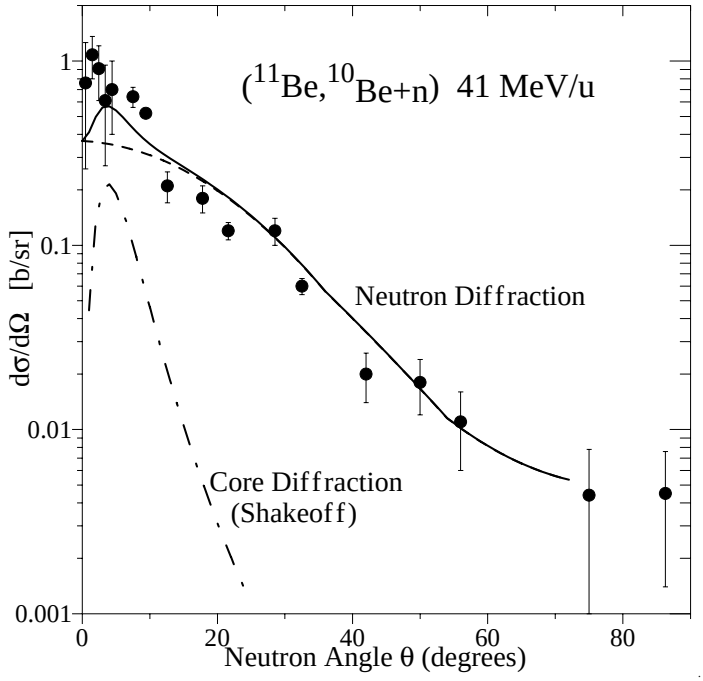

Figure 4. Measured [43] exclusive angular distribution in the laboratory system of neutrons from the reaction ^{9}Be(^{11}Be,^{10}Be+n)X at an incident energy of 41 MeV/nucleon. The theoretical total (full drawn line) is made up of three components. The main contribution arises from diffractive scattering of the neutron [91]. The excess at small angles is due to a combination [95] of shakeoff and Coulomb dissociation, which contribute a total of 16 mb. Inclusion of a finite-size correction (see [81]) would increase this by about 11 mb and would improve the agreement with experiment somewhat.

motion of the core and target, with a lower impact parameter cutoff, but a (nonsudden) quantum-mechanical treatment of the interaction of the neutron with the target. The treatment deals with the diffractive and the stripping parts in a consistent way, and for the longitudinal momentum distribution shown in Fig. 3 it gives results that are very close to those obtained in the eikonal theory.

Only a few experiments have provided direct experimental evidence separating the diffractive breakup of the halo from the stripping reaction. This normally requires detection of the diffracted neutrons in coincidence with the charged residue. The characteristic signature [94] is a broad neutron angular distribution with an opening angle at half maximum of the order of $\theta_{1/2} = 1.6/(kR_T)$, where k is the neutron wave vector and R_T the target radius. The result obtained by Anne *et al.* [43] for the case of ^{11}Be, shown in Fig. 4, is in good agreement with this qualitative estimate. According to theory, the angular distribution of the neutrons has three contributions. The dominant one, calculated by Bonaccorso and Brink [91], is diffraction dissociation contributing 260 mb in good agreement with the experimental value of 240±50 mb. The excess of intensity at small angles is attributed [95] to Coulomb dissociation (9 mb) and to shakeoff (18 mb if a correction for the finite-size effect is included). We will discuss the shakeoff effect in

section 3.2. In an experiment using a silicon multi-detector telescope as an active target, Negoita *et al.* [44] were able to measure separately the elastic-breakup and absorption cross sections as a function of energy. Their inclusive result for 40 MeV/nucleon is shown in Fig. 2.

Most calculations have calculated the cross sections from Coulomb and nuclear dissociation separately and have assumed that they add incoherently. Two new papers go beyond this and apply their findings to the data for Be, Ti and Au targets obtained by Anne *et al.* [43]. Possible interference effects are the subject of the paper by Margueron *et al.* [96], who conclude that they are small but should be detectable. Fallot *et al.* [97] also treat the two interactions together. They follow the time evolution of the halo wave function in a stepwise fashion and and find the large transverse momentum components associated with diffraction at small impact parameters for both heavy and light targets. In these papers [97,98] this effect is also referred to as the "towing mode".

There is considerable experimental evidence showing the existence of proton halos. Reaction cross section data for ^{8}B indicate that it has a significantly extended wave function [99]. Smedberg *et al.* [100] have observed a narrow longitudinal momentum distribution for ^{7}Be fragments from proton removal from ^{8}B. Similar results were found by Kelley et al. [101]. This is a particularly interesting case since the ^{8}B wave function has a strong influence on proton capture in the Sun, which is the source of the high energy neutrinos detected by most solar neutrino detectors on the Earth. This extended wave function has also complicated the interpretation of the Coulomb breakup of ^{8}B since nuclear interactions interfere with Coulomb interactions even at large radius [36,37]. Esbensen and Bertsch [14] use this example to illustrate that the couplings in nuclear-induced breakup of halo nuclei are much too strong to justify the frequently used first-order or truncated coupled-channels calculations.

2.3.3. Reactions of the two-neutron halo

Much effort has been dedicated to the problem of the two-neutron halo, especially to the cases of ^{11}Li and ^{6}He. These are examples of three-body systems with the Borromean property, a term coined by Zhukov *et al.* [24] to denote systems for which the two-body sub-systems are unbound. The fact that, say, ^{11}Li is bound only through the combined effect of the ^{9}Li+n and the n+n interactions led to the expectation that the central-field approximation will fail and that the wave function will show correlations reminiscent of the classic problem of the helium atom in atomic physics. The effects, indeed, turn out to be much more important in the nuclear case. This subject has become too detailed to be discussed in this paper, but we refer to reviews cited above, to other papers in this volume and, especially, to a series of recent theoretical papers by Jensen and his collaborators [9,25,35,95,102–104]. The model developed by these authors starts from a three-body picture. It includes Coulomb and nuclear reaction contributions on an equal footing and it uses a consistent set of parameters to treat all observables.

A central issue has been the angular-momentum components in the two-neutron wave function of ^{11}Li. Measurements of β-decay provided the first evidence for a mixed $s^2 + p^2$ structure, see Refs. [39,40,105,106]. Studies of the two-neutron halo by nuclear reactions were at first difficult because the direct experimental observables in Coulomb and nuclear reactions all are complicated by contributions from the reaction mechanism that

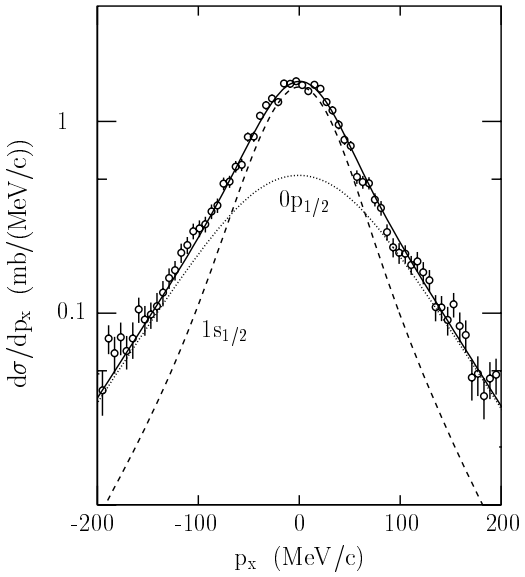

Figure 5. Transverse momentum distribution of ^{10}Li reconstructed from the momenta of ^{9}Li+n in the reaction of ^{11}Li on a carbon target. The decomposition of the distribution into the theoretical l=0,1 distributions is shown. The solid line is a fit corresponding to 45% s^2 in the initial state. (From Simon *et al.* [108].)

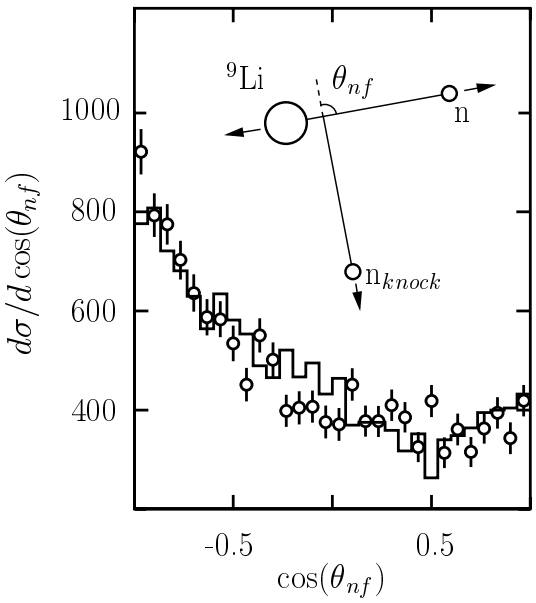

Figure 6. Angular distributions from the decay neutrons measured relative to an axis defined by the ^{10}Li recoil direction as shown in the inset. The points are the experimental data and the histogram is a reconstruction corrected for resolution and acceptance effects. Note the strong forward-backward asymmetry, which reflects the l=0,1 interference. (From Simon *et al.* [108].)

we have only slowly learned to disentangle. An important step in this direction was the paper by Barranco *et al.* [107,75] showing how the transverse momentum distributions are influenced by diffractive and Coulomb effects and by final-state interactions. It is for these reasons that the longitudinal momentum distributions have come to play such an important role in the elucidation of the one-neutron halo, see Fig. 3. These are relatively free from diffractive and Coulomb effects and final-state interactions are absent or very small. The recent paper by Simon *et al.* [108] suggests a new way of attacking the problem of the two-neutron halo. Basically, as applied to ^{11}Li, the idea is to reconstruct the combined momentum of the ^{9}Li+n residue in a stripping reaction on a light target. This directly relates to the momentum distribution of the stripped neutron in the same way as that of the core recoil from stripping of a single-neutron halo. The shape, shown in Fig. 5 can only be fitted with a superposition of $s^2 + p^2$ components with about 50% of each. (For comparison, the p^2 contribution to the ground state of the helium atom is only 0.5%, see Slater [109].) An additional observable, not studied previously, is the relative phase between the components of the wave function. It was, for the first time, determined directly in the same experiment by observing the angular distribution of the decay products

from the recoiling ^{10}Li (Fig. 6). The strong forward-backward asymmetry demonstrates the interference of the l=0,1 final states in the single-neutron removal reaction. Similar experiments have been carried out for ^{6,8}He by Markenroth *et al.* [110]. The theory of the angular distribution in these experiments has been discussed by Garrido *et al.* [103], who successfully accounted for the forward-backward symmetric angular distribution in ^{6}He and predicted the asymmetry in ^{11}Li.

3. BEYOND THE DRIP LINES AND ABOVE THE PARTICLE THRESHOLD

The nucleon drip lines define the boundaries in the (N,Z) plane where the nucleon separation energy vanishes. Neutron-rich nuclei just inside this limit have few bound states and the rest of the energy spectrum consists of broad continuum eigenstates. For proton-rich nuclei, the threshold effects are often less important since the Coulomb barrier reduces the decay widths. The proton radioactivities, discussed in a recent review by Woods and Davids [111], are actually beyond the drip line. Still, their spectra can be strikingly similar to those of nuclei near the valley of beta stability. As an example, the ground state of ^{141}Ho [112] is represented by the same $\frac{7}{2}^-$ [523] Nilsson orbital that forms the ground states of holmium isotopes at the stability line (A=165). For the neutron-rich nuclei, the continuum states play a much more important role. In the following we discuss this from two different angles. The first is that it is in certain cases possible to explore single-particle structure in the continuum via experiments on resonances and final-state interactions. The second aspect, obviously important for the interpretation of such experiments, is that the nearness of the continuum to bound states leads to threshold effects of a nature that is well known from other areas of physics and that have also been observed for halo nuclei.

The continuum part of the spectrum must also enter into the theory of nuclei near the drip lines, but apart from the following remarks this is outside the scope of this paper. Most often, the continuum states are not explicitly considered in the shell-model description of nuclear structure, but they become important for discussing the outcome of reactions. An example is provided by the deviations in the parallel-momentum distribution shown in Fig. 3, where the explanantion [90] has been given in terms of a coupled-channel calculation involving the ^{10}Be+n continuum in a number of l channels. Another recent example [113] dealing with the problem of radiative proton capture in nuclear astrophysics has considered the coupling of many-particle bound states to one-particle scattering states.

3.1. Single-Particle Continuum States Near the Drip Lines

We consider here methods for studying the structure of nuclear systems that only have a continuous spectrum, and take as a specific example ^{9}Li+n, which has no bound levels. It would clearly be ideal to measure the phase shifts in elastic scattering as a function of energy, but although both species exist as beams, neither is available as a target of sufficient thickness. An alternative is to observe resonances in the (unbound) residual nucleus in two-body breakup reactions, where the the (bound) partner is observed in an inclusive reaction. The reaction ^{11}B(^{7}Li,^{8}B)^{10}Li has been used by Young *et al.* [114] and by Caggiano *et al.* [115], and the approach is also open to radioactive beams. Problems, however, arise if the states involved are broad and do not have resonance character. In

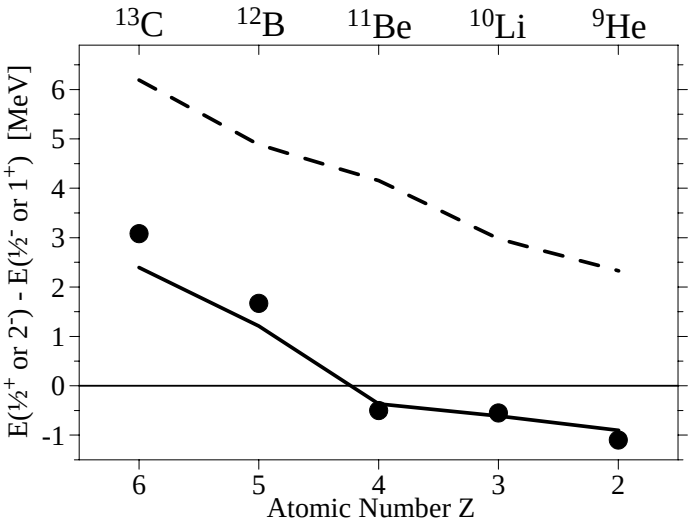

Figure 7. Energy systematics for the the N=7 isotones as a function of the proton number. The difference is taken between the lowest $1/2^+$ and $1/2^-$ levels (even Z) and between the lowest 2^- and 1^+ levels (odd Z). The full drawn curve is the theoretical calculation with the WBT interaction [117,125]. The dashed line shows the result of calculating the level energies within the same model, but without the pairing effect. (This is equivalent to taking the lowest Slater determinant for each spin.) The decrease of 3.3–4.5 MeV in the full model arises mainly from pairing in the p shell, but quadrupole deformations also play a role, especially near the middle of the diagram. The systems ^{10}Li and ^{9}He have no bound states. (Based on [117].)

this situation it is sometimes a solution to investigate reactions in which ^{9}Li+n is formed as a final state. This is usually referred to as the observation of final-state interactions, and is the classical way of studying neutron-neutron, pion-pion, or pion-kaon forces. In the following we give examples of precision studies of this kind performed with radioactive beams. This field is still relatively new.

We take the the N=7 isotones, to which ^{10}Li belongs, as a transparent paradigm of the disappearance of the magic shell gaps in nuclei far from beta stability. Here, an intruder, a $1/2^+$ level from the $1s0d$ shell, is known to appear as the ground state in the last stable nucleus in this sequence, ^{11}Be, as discussed in section 2 and illustrated in Fig. 1. It is clearly interesting to see how this trend continues beyond the drip line in the neutron-unbound systems ^{10}Li and ^{9}He. The current status, including the new data discussed here, is illustrated in Fig. 7. For the two unbound systems, the data and references to the extensive previous work can be found in the recent papers by Thoennessen *et al.* [116] and Chen *et al.* [117].

Structures identified with p-states (and also others) were observed as resonances in the residue. The extensive work on ^{10}Li has been discussed in [116], see the resonance information in [115]. For ^{9}He there are two inclusive measurements reporting a resonance at 1.2 MeV assumed to be the ground state [118–120]. Its relatively narrow width speaks for an l=1 assignment and led to the suggestion [121] that there is no level inversion in

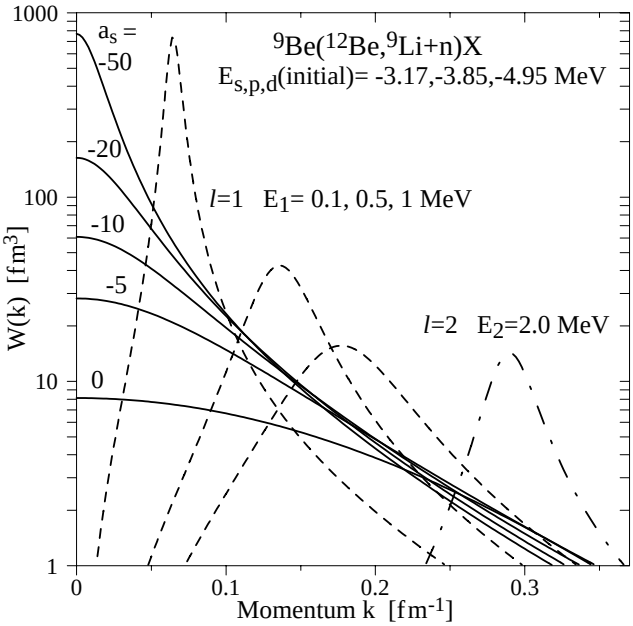

Figure 8. Three-dimensional momentum distributions obtained by expanding the initial state assumed to correspond to a neutron bound in ^{12}Be in continuum eigenstates of the final system. We have chosen an example where the initial nucleus has a substantial population of l=0,1,2 single-particle orbitals. The calculations use Woods-Saxon wave functions for both the initial (bound) and the final (continuum) states, and the results are shown as a function of the three-dimensional wave vector k of ^{9}Li+n. The variable in all calculations is the depth of the potential. It is more transparent, however, to label the states with l=0 (full drawn lines) by their corresponding scattering length a_s (in fm) and the states with l=1,2 by their resonance energies.

this system. The problem is, however, that states with l=0 are more difficult to detect and can easily be missed.

Fig. 8 illustrates why the unbound l=0 states present a special problem in "missing energy" experiments. Unlike the states with l=1,2, they do not exhibit a resonance-like structure, but start with finite probability at momentum $k = 0$ followed by a slow decrease towards higher energies. The resulting line shape is asymmetric with "energy" and "width" roughly comparable [116]. In this case, a Breit-Wigner shape is not a good approximation. The curves in the figure have been obtained by expanding the bound single-particle state (assumed to be a neutron in ^{12}Be) in continuum eigenstates of the final system. The wave functions have been calculated for a Woods-Saxon potential with the radius and diffuseness parameters fixed to 1.25 and 0.7 fm. The depth of the potential in the final system was adjusted to reproduce the resonance energy for l=1,2 (dashed and dot-dashed) and the s-wave scattering length a_s for l=0 (full drawn). Since the initial state does not belong to the same function space as the final states, there is no orthogonality requirement.

A general technique for studying unbound systems that has a good sensitivity to s

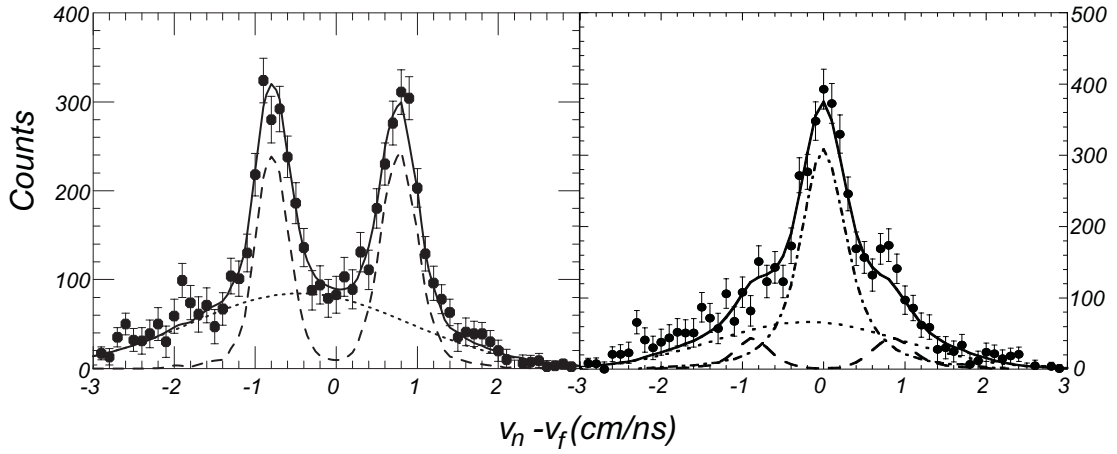

Figure 9. Relative fragment-neutron velocity spectra from the breakup of ^{18}O at an energy of 80 MeV/nucleon. The left panel shows that coincidences with a ^{6}He fragment leads to the characteristic l=1 distribution corresponding to the $0p_{3/2}$ resonance at 450 keV in ^{7}He. The right panel shows coincidences with ^{9}Li+n. The dominant (dot-dashed) contribution is s wave calculated here for a scattering length a_s of -30 fm corresponding to the ground state of ^{10}Li. The dashed component is the contribution from an assumed l=1 state at 540 keV. The dotted curves in both panels are an estimated background contribution arising from highly excited intermediate states. (From [116]).

states has been developed by Thoennessen, Galonsky and their collaborators [116,122]. Based on exclusive measurements of fragments and neutrons emerging from reactions in a light target, it detects the final-state interaction of the system of interest. The example shown in Fig. 9 illustrates how it identifies the dominant states of ^{7}He and ^{10}Li.

In a recent extension [117] of this work, direct reactions of radioactive projectiles have been used to populate the continuum states. Selection rules can then be used for linking the angular momentum of the initial state to that of the final state. Instead of ^{12}Be, as in Fig. 8, it is possible to choose the projectile ^{11}Be, where the valence neutron is predominantly in the $1s_{1/2}$ state. This creates a situation where the single- and double-proton knockout leading to ^{10}Li and ^{9}He will favor just this neutron orbital. Both reactions showed a strong final-state interaction in the l=0 channel indicating a low-lying s state. The analysis was based on the sudden approximation. The theoretical distributions were obtained by expanding the initial bound neutron state similarly to the example shown in Fig. 8. The analysis for ^{10}Li confirms the result of [116] of a neutron scattering length a_s more negative than -20 fm. For ^{9}He the limit is -10 fm. For the comparison with the energies of resonances in Figs. 7 and 10 it is convenient [117] to take as an operational definition the relation $E = \hbar^2/(2\mu a_s^2)$, where μ is the reduced mass. Following Landau and Lifshitz [123], one arrives at this by noting that for bound states, just below and very close to the threshold, the eigenenergy is given by exactly the same expression but with opposite (negative) sign. Consequently, the energy of the virtual state in ^{9}He is less than 0.2 MeV. This is well below the 1.2-MeV resonances previously assumed to represent the ^{9}He ground state and demonstrates that the parity inversion persists beyond ^{11}Be and ^{10}Li.

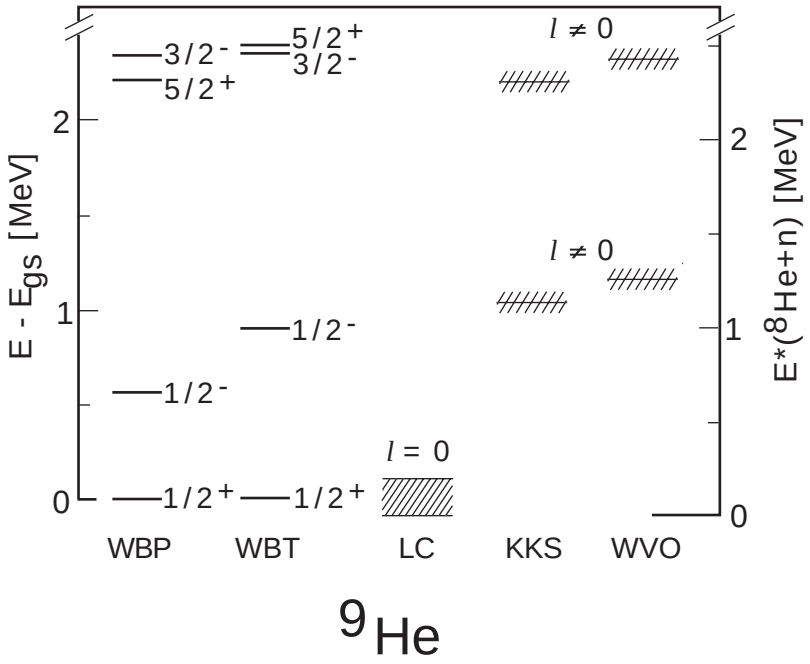

Figure 10. Level scheme of ^{9}He. Theoretical calculations with the WBP and WBT interactions of Warburton and Brown [125] are compared with the final-state interaction experiment marked marked LC [117] and previously reported resonances in the ^{8}He+n exit channel marked KKS [118] and WVO [119,120]. The currently cited ground-state mass for ^{9}He is based on the resonance near 1.2 MeV.

Fig. 10 shows all data for this system and compares with a shell-model calculation for the $0p$-$1s0d$ space based on the WBP and WBT interactions [124,125]. These calculations assume that the continuum eigenstates may be approximated by discretized bound states obtained in a calculation based on effective interactions.

The excellent agreement between experiment and theory suggests that it is possible to perform an "autopsy" on the calculation [117] in order to learn the reason for the level crossing. By restricting the configuration space to $[(0p_{3/2})^4, 0p_{1/2}]$ and $[(0p_{3/2})^4, 1s_{1/2}]$ for the $1/2^-$ and $1/2^+$ states, respectively, one obtains the equivalent to performing a spherical Hartree-Fock calculation (with no pairing). In this approximation, the level crossing disappears, and the energy of the $1/2^+$ state is increased by 3.3 to 4.5 MeV in all N=7 isotones. The result, shown in Fig. 7, demonstrates shows that the lowering of the state in the full model is a result of pairing and deformation. This contradicts the notion that intruder states are caused alone by a change in the single-particle energies with neutron and proton number. In section 4.1, we shall encounter a more developed pairing wave function, bridging the p and sd shells, for the case of the N=8 nuclide ^{12}Be.

Experiments carried out at the GSI have also found evidence for low-lying s strength in ^{10}Li, both from the angular distribution in the (^{11}Be,^{9}Li+n) [126] and from a reconstruction of the invariant mass in the (^{11}Li,^{9}Li+n) reaction [127]. The former experiment favors a neutron scattering length of the order of -20 fm or more negative. The analysis of the breakup has been discussed by Bertsch *et al.*, [128] who find evidence for strong

$s^2 + p^2$ mixing in ^{11}Li, in good agreement with the discussion in Sect. 2.3.3.

It is clearly interesting to examine the Z=7 isotopes to see if a similar inversion will appear in ^{11}N, the mirror nucleus of ^{11}Be. In the neighbor ^{12}N, the doublets associated with the $\frac{1}{2}^+$ and $\frac{1}{2}^-$ proton states are already close. (The systematics of the level energies for the corresponding isotones has been shown in Ref. [129].) Several recent papers [130–132] present evidence that the $\frac{1}{2}^+$ is lowest in ^{11}N, approximately 1.3 to 1.6 MeV above the particle threshold and 0.5-0.8 MeV below the $\frac{1}{2}^-$ resonance. According to Sherr [133] this is in excellent agreement with what should be expected from the systematics of the Coulomb shifts in the A=11 isospin quartet. The papers cited give references to earlier work and to some theoretical papers. The experiments offer instructive examples of the main techniques for studying continuum states discussed in the beginning of this section. Azhari *et al.* [130] used the direct rection ^{9}Be(^{12}N,^{10}C+p)X at 40 MeV/nucleon and reconstructed the energies of the excited continuum states. The experiment of Oliveira *et al.* [131] observed the spectrum of ejectiles in the reaction ^{10}B(^{14}N,^{13}B)^{11}N and obtained levels using two-body kinematics. Finally, Markenroth *et al.* [132] measured elastic scattering of a radioactive ^{10}C beam on a proton target and observed resonances in the joint system. (This is the reaction that is technically impossible in the mirror system.)

The experiments discussed here illustrate that it is possible to identify single-particle structure in nuclei beyond the neutron drip line or above the particle threshold. The broad, unspecific structures, however, make the experiments difficult. It is clear that experiments involving two unbound particles will be even harder, since they have one more dimension in the coupling than in Fig. 8. Furthermore, the drip-line nuclei will often have a bound level very close to threshold. This leads to other complications that affect the analysis of experiments. We discuss these effects in the following section.

3.2. Threshold and Continuum Effects in Reactions of Nuclei Near the Drip Lines

A halo state is situated just below a particle-core threshold, and it is not surprising that there is an interplay with continuum states with the same quantum numbers existing just above the threshold. In fact, we may think of the tail developing in the halo wave function as a gradual approach to the continuum states existing above zero energy, see Fig. 1. This interplay will manifest itself in reactions in which the halo state is created. In this case the cross section will show a sharp peak at negative energy and a broad and (usually, but not necesssarily) weaker "ghost peak" at positive energies. This general phenomenon has been discussed by Barker and Treacy [134]. A good example is provided by the reaction ^{9}Be(p,d)^{8}Be, where the 0^+ ground state is quasi-bound. Just above the $\alpha - \alpha$ threshold an asymmetric peak at 0.6 MeV with a "tail" towards higher energies appears in experiments [135]. The peak, which could tempt an interpretation as a structural effect, can be shown in an R-matrix analysis to be the same state as that which produces the narrow ground state. A condition for this is that the channel at the threshold has an appreciable spectroscopic factor with respect to the bound state.

Atomic and x-ray physics and their boundary area to nuclear physics offer many examples of processes that change the average electrostatic environment of the atom. Examples are the production of an inner-shell vacancy in a photoelectric process, in (e,e') scattering, or in internal conversion. The removal of a unit charge inside the atom modifies

the potential in which the other electrons move. Usually the change can be regarded as instantaneous, so that the sudden approximation is applicable. The new eigenfunctions are not orthogonal to those of the initial system, and although the overlap still is good, there is now a certain probability that electrons will be excited. For a single-particle excitation in a central potential, the possible final states are bound and unbound states having the same angular-momentum quantum numbers. In atomic physics one traditionally refers to "shakeup" when speaking of excitations leading to bound states, and to "shakeoff" for excitations leading to the continuum. A number of examples, mainly seen from the viewpoint of atomic physics, are discussed in a book edited by Crasemann [136]. The interplay with the atomic electrons in nuclear reactions is the subject of a review article by Freedman [137]. The ejected electron can sometimes be observed directly, and in other cases the vacancies in the filled shells give rise to "satellite lines" in x-ray and Auger-electron spectra.

A particularly simple example is nuclear $\beta^{\pm}$ decay, which changes the nuclear charge by one unit. The effect on the atomic shell is appreciable: some 20-30% of the atoms [137] will undergo shaking, almost independently of Z. Beta decay by K-shell capture, on the other hand, conserves the charge at the atomic center and has much weaker satellite excitations in the primary process. The atomic excitation spectrum in the beta decay of tritium has attracted a good deal of interest, see *e.g.* [138], because of the importance of this process for measurements of the mass of the electron anti-neutrino.

It is clear that a halo state, which is a kind of "nuclear atom", also must be expected to show shakeup and shakeoff effects. These are caused by nuclear scattering or reactions involving the core with the loosely bound halo particle present as a spectator. The excitation of the spectator may be viewed as a side effect, so to say as collateral damage accentuated by its weak binding in the initial (or final) state. The simplest case, completely analogous to the shakeoff in beta decay, is a reaction in which a spectator neutron has the separation energy S_1 in the initial state and S_2 in the final state. Assuming that the projectile velocity is much greater than the internal velocity of the neutron, the sudden approximation gives the survival probability of the final state

$$P_{12} = |\int d\vec{r}\,\psi_1^*(\vec{r})\psi_2(\vec{r})|^2 \approx \frac{4\sqrt{S_1 S_2}}{(\sqrt{S_1}+\sqrt{S_2})^2}, \tag{6}$$

where the right-hand approximation is based on Yukawa wavefunctions and hence is valid only for s states. An example of this effect is provided in the single-neutron knockout (^{12}Be,^{11}Be) [139], which will be discussed in more detail in section 4. For the reaction to the l=0 ground state, the approximation given in the right-hand side of equation (6) leads to a probability of 0.82 while a more accurate Woods-Saxon calculation gives 0.79. For the p states in the same reaction the value is 0.83. The effect is big enough to influence the measurements of absolute spectroscopic factors. The missing part of the cross section should be detectable as a broad continuum in ^{10}Be+n at low energies.

Another class of processes in atoms, solids and nuclei involve excitations and breakup following the transfer of of momentum. For a two-body system with relative coordinate $\vec{r}$, the sudden transfer of a momentum $\vec{q}$ in the new center-of-mass system attaches a phase $\exp(i\vec{q}\cdot\vec{r})$ to the wave function. The overlap with the original ground state, called a form

factor, is

$$F(\vec{q}) = \int d\vec{r}\,|\psi_0(\vec{r})|^2\,\exp(i\vec{q}\cdot\vec{r}). \tag{7}$$

The square of this gives the probability that the state is not excited in the process. The best known example of this phenomenon is the recoilless emission of photons in the Mössbauer effect, see [140]. In solid-state physics, the probability of not exciting lattice phonons is referred to as the Debye-Waller factor. There are a number of cases in which shakeoff following a momentum transfer in nuclear collisions plays a role. Although one usually does not think of it this way, E1 Coulomb dissociation at intermediate energies is actually a perfect example. During the brief collision time, the Coulomb impulse $\vec{q}$ sets up a new state as discussed in connection with equation (7). For small $\vec{q}$, the main process is elastic scattering with a small probability of breakup. In this limit, the dipole approximation is valid. For the case of a well-developed halo in an s state such as ^{11}Be, we may approximate the initial state by a Yukawa wave function and the final state by plane waves. The resulting distribution of the reduced transition probability is then approximately [47,141]

$$\frac{dB_{1n}(E1)}{dE} \propto \frac{E^{3/2}}{(S_{1n}+E)^4} \tag{8}$$

where E is the kinetic energy of the final state and S_{1n} the neutron separation energy. This formula gives an excellent description of the ^{11}Be case, as can be seen from the comparison with the experimental data of Nakamura *et al.* [56] shown in Fig. 11.

It is characteristic that the shape of the spectrum to lowest order does not depend on the absolute magnitude of the momentum transfer $\vec{q}$, but only on the the parameter S_{1n} of the initial state. (The absolute shakeoff probability, however, depends on q^2.) A consequence is that all scattering angles contribute with the same spectrum. This is, of course, just another way of expressing the sum rule result Eq. (3), which links the average energy of the final states directly to the binding energy of the initial state. In the words of Esbensen and Bertsch [53], "the dipole operator does not change the momentum content much". The same distribution will show up in other collision processes in which the halo neutron is a spectator. One example is the shake-off peak seen at small angles in the neutron angular distribution in Fig. 4. Another example is the elastic scattering of ^{11}Be on a carbon target, where the effect, in principle, should be observable indirectly as missing intensity at large angles. According to theory [142], this decrease in $d\sigma/d\Omega$ can be traced back to a form factor like the one discussed above.

Equation (8) describes Coulomb excitation or shake-off from a one-neutron halo system in an s state and in the absence of final-state interactions. Pushkin *et al.* [141] have used a three-body model to derive the corresponding expression for the case of a two-neutron halo dominated by components with hypermomentum K=0 and with final states that are plane waves. They obtain an exact expression in terms of special functions, which to a good approximation can be simplified to

$$\frac{dB_{2n}(E1)}{dE} \propto \frac{E^3}{(1.5S_{2n}+E)^{11/2}}, \tag{9}$$

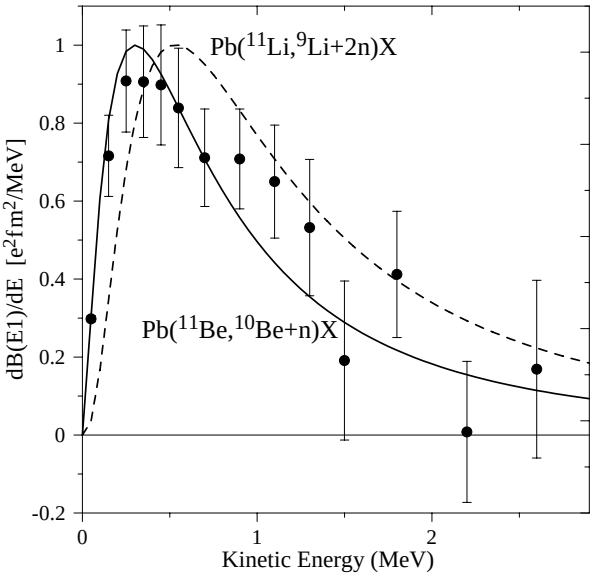

Figure 11. Distribution of the reduced E1 transition probability. The points represent the experiment for ^{11}Be [56]. The full drawn curve is equation (8) calculated for a neutron separation energy of 0.503 MeV. For convenience, the dashed line shows the corresponding three-body expression, Eq. (9) given by Pushkin *et al.* [141], and calculated for a two-neutron separation energy of 0.30 MeV corresponding to the case of ^{11}Li.

which is in excellent agreement with the experiment on ^{11}Li by Shimoura *et al.* [57]. The corresponding distribution is shown in Fig. 11. Again it appears that the same distribution has been detected in inelastic proton scattering, where a peak was observed [67] at a kinetic energy of 1.0 MeV (or 1.3 MeV excitation energy measured from the ^{11}Li ground state). An interpretation in terms of shakeoff [68] can account for the absolute cross section, the angular distribution and the fact that the same spectrum appears at all angles. It is, of course, perfectly possible that the observed broad distribution has contributions that go beyond this simple picture and also that other mechanisms contribute.

A different case is presented by the two-neutron halo of ^{6}He, which has the neutrons in p states and is considerably more bound than ^{11}Li. A number of different reactions producing ^{4}He+2n as a final state, see *e.g.* [143,144], all show a broad distribution with a peak at low excitation energy and a tail toward higher energies. In addition, the well-known 2^+ resonance shows up in as a sharp peak below the continuum. The "background" peak in invariant-mass spectra has been investigated by Forssen *et al.* [145]. Using a three-body model dominated by hypermomentum $K = 2$, they reproduce the shape of the asymmetric peak quite well. This peak, in their words, is nothing but a reflection of the ^{6}He ground state, and it closely resembles what is obtained in an estimate of shakeoff.

3.3. General remarks on the spectroscopy of unbound nuclei

The upshot of this section is then, as discussed in section 3.1, that it is sometimes possible to observe features of nuclear structure in regions of the nuclear chart where there are no nuclei, properly speaking. The proton radioactivities are a poster example of this.

More tenuous, but still possible, is the identification of scattering parameters corresponding to single-particle motion of an unbound neutron. Such information may be essential for understanding two-neutron halos such as in ^{11}Li, ^{14}Be, and, with time, in heavier nuclei. On the other hand, it is important to be aware that the broad continuum structures of very neutron-rich systems are treacherous ground. Other mechanisms discussed in section 3.2 enter, and it may become difficult to decide from simple arguments whether a given continuum distribution, especially at low energy, is chaff from the reaction or a clue to the structure.

We have shown examples where a low-energy peak is just the reflection of a subthreshold bound state. In such cases, low-momentum continuum components are generated that are very similar those present in the bound state. It appears that this holds, irrespective of whether they are produced in an excitation of the state at threshold or produced in some other reaction where the state is not present initially. The broad peaks in Coulomb excitation, given theoretically by the approximations (8) and (9), emerge in a model with no structure in the final states, which are represented just by by plane waves.

The problems must be exacerbated in three-body systems, where the behavior of the three-body continuum is far from being simple, see [146]. Taking the example of the continuum above the two-neutron threshold in ^{11}Li, it is probably too simplistic to interpret it either as due to shakeoff or as an excited state with spin and parity 1^-. Both interpretations are actually be built on the same basic ingredients, which are the continuum single-particle states with $l = 0, 1$ in ^{9}Li+n. Closer scrutiny of the ghost state will almost certainly reflect finer details carrying information on the interactions in the exit channel. The fundamental question is more whether the structural information that can be gathered in this way is worth the effort.

The problem of identifying states and measuring energies in unbound systems is, however, more than just a difficult exercise in nuclear spectroscopy. Measured total binding energies of nuclear states serve as an important check on the validity of very basic theoretical calculations. The advanced many-body theory of shell structure is currently able to handle nuclei in the region near mass 10, see [147,148], and the experimental masses serve as benchmarks. As an example, consider three experiments, based on quite different techniques, that have reported the observation of the lowest state of ^{10}He, unbound towards ^{8}He+2n. In proton stripping on ^{11}Li, Korsheninnikov *et al.* [149] found a peak at 1.2 ± 0.3 MeV by reconstructing the excitation energy of the three final products. Another experiment [150] measured the reaction ^{10}Be(^{14}C,^{14}O)^{10}He assumed to represent two-body kinematics and found a peak with marginal statistics at an energy above threshold of 1.07 ± 0.07 MeV. A third experiment based on a (p,2p) reaction [151] found an energy of 1.7 ± 0.4 MeV. However, the energy of about 1.1 MeV is also roughly the energy that the momenta of ^{8}He and the two spectator neutrons would add up to, were we dealing with an initial-state effect. The experiments are behind the ground-state mass cited for ^{10}He in the latest mass evaluation [152], but further evidence for the true resonance character of this state is desirable. (See also the discussion of ^{9}He in Fig. 10.)

4. SPECTROSCOPY OF BOUND STATES BY SINGLE-NUCLEON KNOCK-OUT REACTIONS

The single-nucleon transfer reactions observed with high resolution at beam energies typical of early cyclotrons and van de Graaf accelerators were of great importance for developing our understanding of nuclear structure. They directly identified l values and single-particle occupancies of the nuclear wave function [153–155]. Typical examples are the stripping and pickup reactions, (d,p) and (p,d), respectively, but many other reactions have been used including two-particle transfers. It is possible to extend this method to radioactive beams, see the recent work on the p(^{11}Be,^{10}Be)d reaction at 35 MeV/nucleon studied by Fortier *et al.* [156,157] and the d(^{56}Ni,^{57}Ni)p reaction studied by Rehm *et al.* [158]. There is also an interest in applying transfer reactions for investigating structure in the continuum, a problem closely related to the discussion in Sect. 3.1. In a new experiment, Korsheninnikov *et al.* [159] have used the reaction p(^{8}He,^{7}He)d for observing an excited state at 2.9 MeV in the unbound residue ^{7}He.

In the following we discuss a new technique, based on in-flight separated beams from fragmentation reactions, typically at energies above 50 MeV/nucleon. In this method the projectile residues from single-nucleon removal are observed in inverse kinematics with a high-resolution spectrograph. The final states of the heavy residues are identified by their gamma decay. This method has, so far, been applied to the projectiles ^{26,27,28}P [16], ^{11}Be [46], ^{12}Be [139], ^{14}B [160] and ^{15,16,17,19}C [161,162]. The partial removal cross section determines the spectroscopic factor while the shape of the longitudinal momentum distribution determines the orbital angular momentum l. A few examples from this work are given below. We refer to this process as a knockout reaction[2] to emphasize the relationship to the classical (p,2p) reactions, see [164], in which the recoil momentum of the heavy residue was reconstructed from the momenta of the two outgoing protons. In inverse kinematics, the momentum of the residue is observed directly.

4.1. Theory and Experimental Results

It was pointed out early by Sagawa and Yazaki [165] that the observed inclusive momentum distribution of residues from the (^{11}Be,^{10}Be) reaction on a light target will contain broad contributions from core knockouts leading to bound excited levels in ^{10}Be. For this it is necessary that the halo neutron will remain attached to the residue. Estimates show that the shakeoff probability is low (less than 10%), see [166]. The core contributions, which amount to 22% have recently been observed experimentally [46] by a gamma-ray coincidence technique. By observing neutron-fragment coincidences it should, in principle, be possible to extend this method to excited continuum states in experiments resembling those discussed in Sect. 3.1.

In a parallel theoretical development it has turned out that the methods based on Glauber theory developed for halo states, see section 2.3, have a wider applicability. Over the past couple of years, a number of experiments involving both halo and more bound

[2] Another term appropriate for an essentially instantaneous nucleon removal process would be "stripping", coined by Serber in 1947 to describe the nuclear breakup of 190 MeV deuterons [163]. (It implicitly refers to a procedure in weapons technology.) However, this word with time has come to be used instead for transfer processes. In the present paper, we occasionally use it in the original meaning such as in connection with equation (5).

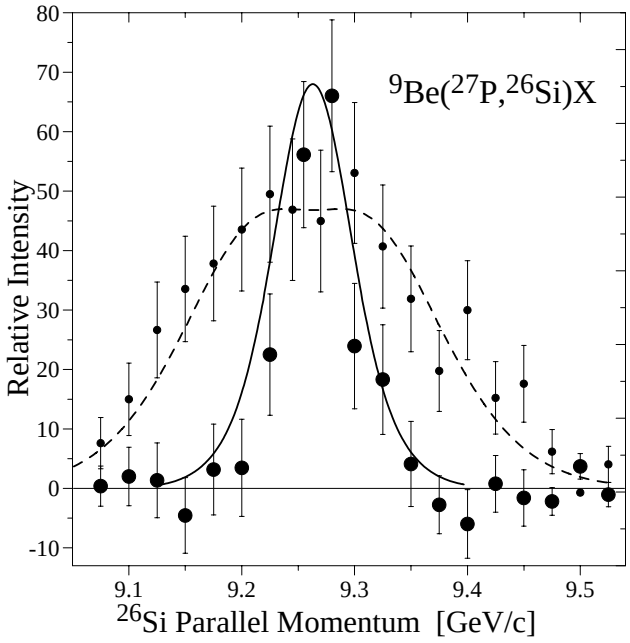

Figure 12. Momentum distributions for the ^{9}Be(^{27}P,^{26}Si)X reaction to the ground state (large circles) and all excited states (small circles). The corresponding theoretical curves in arbitrary normalization are calculated in the eikonal theory. The full-drawn line corresponds to l=0 and the dashed one to l=2. (From [16].)

"normal" states have been carried out. For the analysis of these experiments it is assumed [83] that the partial cross section $\sigma_{th}(I^{\pi})$ for populating a given final state I^{π} of the residue can be written

$$\sigma_{th}(I^{\pi}) = \sum_{j} C^2S(I^{\pi}, nlj)\sigma_{sp}(S_n, nlj), \tag{10}$$

where C^2S is the spectroscopic factor for removal of a nucleon with given single-particle quantum numbers (nlj). This quantity has been taken from many-body shell-model calculations by Brown and his collaborators [124,125,167], and it expresses the parentage of the initial state with respect to a specific final state. The sum in Eq. (10) is taken over all configurations which have a nonvanishing parentage. The σ_{sp} are the single-particle removal cross sections, which are strongly dependent on the orbital angular momentum l and the nucleon separation energy S_n. The calculation of these quantities in an extension of Glauber theory has been discussed by Tostevin in [83,90], and the basic expressions were given in equations (4) and (5).

As an example, we take a study of the proton-rich isotopes of phosphorus [16] which, as discussed in section 2.1, are interesting candidates for ground-state proton halos [15]. The isotopes ^{26,27,28}P are expected to have a dominant contribution of the $1s_{1/2}$ proton orbital, and their proton separation energies of 0.14 ± 0.20, 0.897 ± 0.035 and 2.066 ± 0.004 MeV, respectively, are low. The results [16] for the case of ^{27}P are shown in Fig. 12. The low counting statistics for the gamma spectrum made it necessary to resort to a gamma-ray tagging technique which divides the fragment data into two sets corresponding to

coincidences and anti-coincidences with gamma rays. This requires knowledge of the average detection efficiency, $54 \pm 5\%$, estimated from the theoretical level scheme. The spectra also had evidence for a structureless continuum distribution with an intensity of $10 \pm 5\%$ above 0.25 MeV integral bias. This is attributed to neutrons, charged particles and γ rays produced in the target and to their secondary interactions with construction materials and the scintillator. (Later work [139,161] has given more accurate estimates of this component but confirms the analysis in [16].) The measured gamma branching ratio of $30 \pm 10\%$ to the ground state corresponds to a partial cross section of 22 ± 8 mb, which translates into a $1s_{1/2}$ spectroscopic factor of 0.46 in excellent agreement with the theoretical spectroscopic factor obtained in the shell-model calculation. From the figure it is clear that the cross section to the ^{26}Si ground state is l=0 thus proving that the ground state of ^{27}P has spin and parity $1/2^+$. The figure also shows that the cross sections to the ^{26}Si excited levels are predominantly l=2 in agreement with theory. Similar results were found for other light phosphorus isotopes.

On theoretical grounds, and backed by some experimental evidence, it is assumed [168] that neutron-rich nuclei near the drip line may show a shifting and even vanishing of the magic shell gaps. We use as our second example an experiment by Navin *et al.* [139] bearing on this question. In the case of the N=8 nucleus ^{12}Be, indirect evidence, based on analogue displacement energies and reaction data, had long ago made Barker [169] suggest that intruder states would play an important role. This was also found in the recent analysis by Sherr and Fortune [170], but contrasts with the properties of the even-even neighbor with 8 neutrons, ^{14}C, which is very magic. The experiment [139] provided a direct measurement of the composition of the wave function in the knockout reaction ^{9}Be(^{12}Be,^{11}Be)X leading to the ground state and (only) excited state, see Fig. 1. For an N=8 closed neutron shell the spectroscopic factor to the excited level should be close to 2 corresponding to a filled $0p_{1/2}^2$ level.

Although the gamma spectrum showed a strong 320 keV gamma ray, the corresponding absolute cross section was only one quarter of that expected for a closed shell. The spectroscopic factor is 0.45 ± 0.07 after correction for an imperfect overlap of the type discussed in connection with equation (7). The error is purely experimental. Subtraction of the gamma-coincident part from the inclusive cross section shows that approximately two thirds of the cross section goes to the $1/2^+$ ground state corresponding to a very similar spectroscopic factor, 0.53 ± 0.07. The missing spectroscopic factor relative to the simple sum rule (that would give about two) must come from the $0d_{5/2}$ state, which is unbound and therefore could not be observed. This experiment is a direct demonstration of the breakdown of the N=8 shell closure and shows a pairing-type wave function with comparable $s^2 + p^2 + d^2$ components characteristic of a deformed nucleus. The deformed character of ^{12}Be finds support in two recent experiments by Iwasaki *et al.* [171], who find that inelastic proton scattering indicates a strong quadrupole deformation of the neutrons and also, with a heavy target, a strong E1 excitation to a 1^- level at only 2.68 MeV and with a B(E1)=0.05 e^{2}fm^2, see the similar example in Fig. 1. The ^{12}Be experiment raises the question whether the neutron halo of the N=8 neighbor, ^{11}Li, also has a significant $0d_{5/2}$ component. This was not considered in the analysis used in Ref. [108].

The case of ^{17}C, taken from an extensive series of experiments on the neutron-rich isotopes of carbon by Maddalena *et al.* [161] provides a good example of what can be

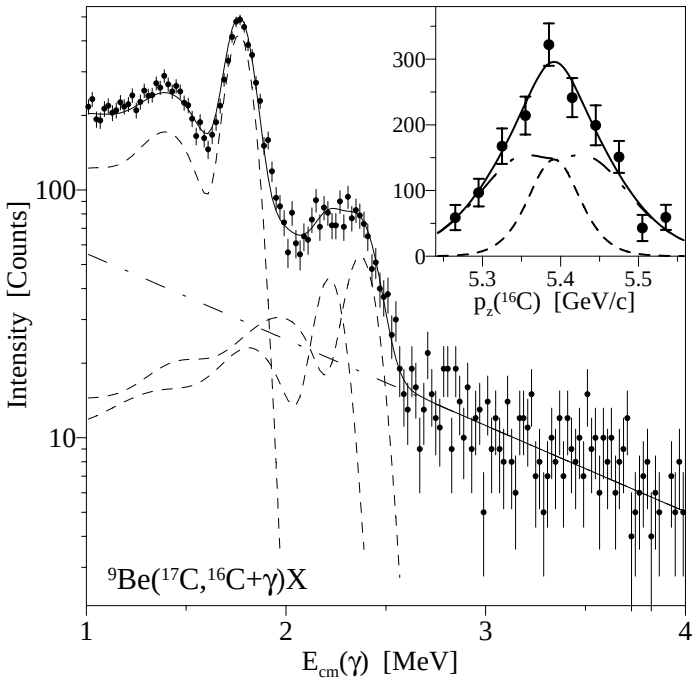

Figure 13. Doppler-corrected γ-ray spectrum measured in ^{9}Be(^{17}C, ^{16}C+γ)X. The full-drawn curve is a fit to the spectrum with the individual γ components shown as dashed lines. The peak at 1.77 MeV shows that about half of the cross section goes to the first-excited 2^+ level. The inset shows the parallel momentum distribution of the projectile residues feeding the 1.77 MeV level directly. The fit requires a superposition of l=0 (dashed) and l=2 (dot-dashed) contributions. (From [161])

achieved with the knockout technique. Key data from this experiment are shown in Fig. 13. A detailed analysis, which we omit here, provides a firm $\frac{3}{2}^+$ assignment for the ^{17}C ground state, which is interesting for being based essentially on the the wave function of the 2^+ excited level at 1.77 MeV in ^{16}C [172] . The strong gamma ray in Fig. 13 shows that this level receives about half of the cross section. Two main components in the wave function of the $\frac{3}{2}^+$ ground state are revealed in the parallel-momentum distribution shown in the inset of Fig. 13. The main one is $0d_{5/2} \otimes [0d^2_{5/2}]_{2^+}$ which gives $l = 2$ knockout. A smaller admixture of $1s_{1/2} \otimes [0d^2_{5/2}]_{2^+}$ gives the $l = 0$ component. The theoretical cross sections calculated from equation (10) of 12 and 53 mb for l=0,2, respectively, agree very well with the experimental values of 16 ± 7 and 44 ± 11 mb. This is a a striking demonstration of the possibilities of the knockout method and of the power of shell-model theory in the region of the p–sd shells.

It will be interesting to see this method extended beyond the $p - sd$ shells to heavier nuclei and, in particular, to those with a large neutron excess. This will become possible with the radioactive-beam facilities that are now being prepared. It is almost certain that better experiments will reveal new features of the method as well as a need for refinements. Some early examples of this have been mentioned above. One open question is how the method will apply to nuclei with strong permanent deformations. A first case [16] of

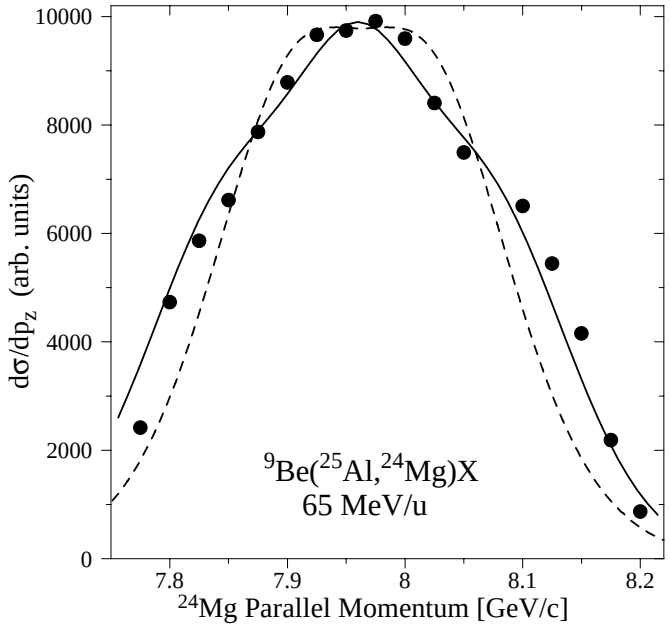

Figure 14. Longitudinal momentum distributions in the knockout reaction (^{25}Al,^{24}Mg). The points are the experimental inclusive data taken at 65 MeV/nucleon [16]. The calculation for a spherical l=2 state (dashed) in [16] gives a poor description of the shape. The theory (full drawn) of Sakharuk and Zelevinsky [173] calculates the spectra to the ground-state rotational band in the Nilsson model assuming a $\frac{5}{2}^+$ [202] ground state of ^{25}Al. It succeeds in accounting for the characteristic "shoulders", which it is tempting to view as reflecting the transverse and longitudinal components of the particle momentum in the deformed field.

a reaction connecting two deformed nuclei is (^{25}Al,^{24}Mg), see the inclusive momentum distribution shown in Fig. 14. Sakharuk and Zelevinsky [173] investigated this general problem applying the Nilsson model for calculating the knockout of a (deeply bound) proton to the $0, 2, 4^+$ members of the ground state rotational band. They found very different shapes of the distribution for the three components as well as a characteristic intensity pattern. It is very likely that reactions of deformed projectiles will offer a rich source of specific information resembling the "fingerprints" seen in transfer reactions at low energy on rare-earth nuclei [153].

4.2. How accurate are the knockout reactions as a spectroscopic tool?

The results obtained by the knockout method are, so far, very promising. However, there is no reason to expect exact agreement between experiment and equation (10), which is a heuristic link between two unconnected theories. In order to test this relation experimentally, we define a scale factor F as the ratio between the experimental and the theoretical cross section. The scatter in F is then a test of the overall validity of this approach, while the average of F conveys information about possible empirical renormalizations. This would be analogous to the effective charges and effective coupling constants discussed for the *sd* shell by Brown and Wildenthal [124].

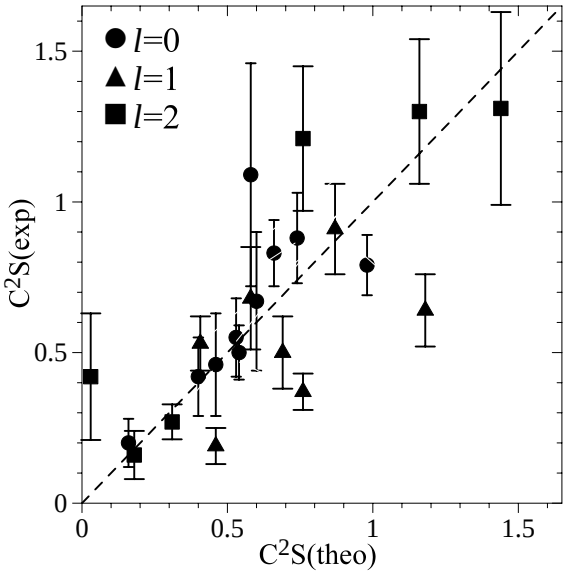

Figure 15. Comparison of experimental and calculated spectroscopic factors for reactions at approximately 60 MeV/nucleon leading to individual final levels in the nuclei ^{25,26,26}Si, ^{10,11}Be, ^{13}B, and ^{14,15,16,18}C [16,83,46,160,139,161]. Circles, triangles and squares correspond to l=0,1,2, respectively. The dashed line corresponds to F=1.

The nuclear-structure part of the theory has been eminently successful for nuclei up to mass 40, and we have much confidence in its predictions. Still, it is useful to recall that it is in some way a caricature of a real nucleus. It defines the spectroscopic factors in a severely truncated Hilbert space with nucleons assumed to be the fundamental building blocks. These are subject to effective interactions with strengths chosen to compensate for the neglected degrees of freedom. The reaction theory is less well proven experimentally. It starts from a picture of quasi-free nucleons, generally believed to be valid at considerably higher energies, and with key input parameters taken to be nucleon densities and (free) nucleon-nucleon scattering cross sections. Tostevin [83,90,162,174] has performed calculations based on other reaction models and has provided a substantial theoretical underpinning of the theoretical single-particle cross sections, which may be accurate to $\pm 20\%$. All results cited here are based on common, pre-existing parameter sets and individual adjustments have been avoided.

Two sets of data are, at the present time, available for comparisons. The experiments discussed in section 4.1 have measured l values and spectroscopic factors for 24 individual partial cross sections for proton and neutron removal reactions in the p and sd shells. The comparison of experimental and theoretical spectroscopic factors given in Fig. 15 suggests an good overall agreement. Leaving out 5 cases with theoretical spectroscopic factors smaller than 0.4, we calculate the average scale factor $\langle F \rangle$ separately for each l value. For the nine l=0 partial cross sections we obtain $\langle F_0 \rangle = 0.99 \pm 0.07$ with a χ^2 per degree of freedom of 1.1. Seven cases with l=1 give $\langle F_1 \rangle = 0.61 \pm 0.10$ where the (compound) experimental error has been scaled with the square root of the χ^2 per degree of freedom of 3.4. Finally, three l=2 partial cross sections give $\langle F_2 \rangle = 1.1 \pm 0.3$ with a

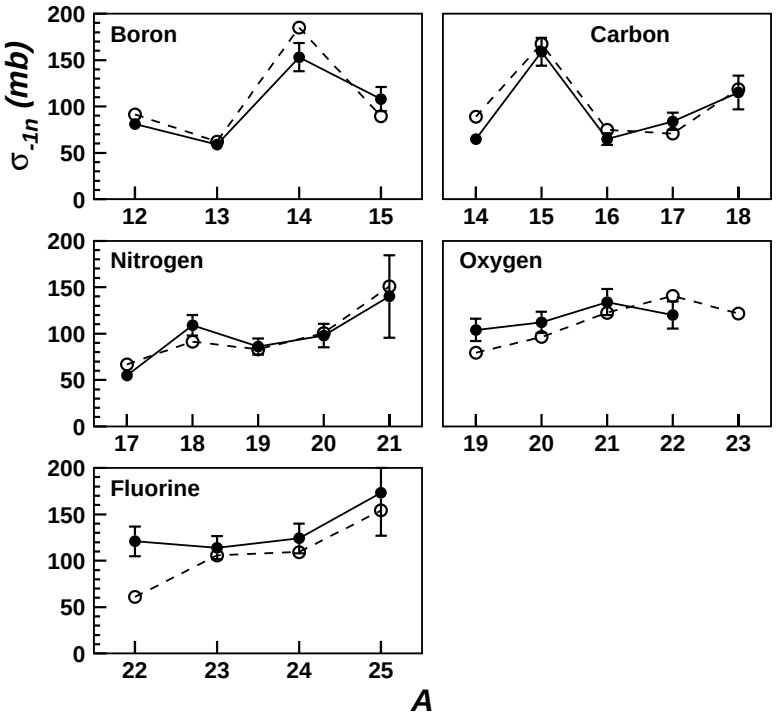

Figure 16. Measured (solid points) and calculated (open points) inclusive one-neutron removal cross sections measured at a constant magnetic rigidity setting corresponding to energies of 43-71 MeV/nucleon. (From Sauvan *et al.* [175])

a χ^2 per degree of freedom of 1.6. The low value for l=1 may reflect contributions from high-lying $0^-, 1^-$ levels situated close to the neutron threshold in even-even nuclei.

A second test comes from a recent experiment carried out at GANIL by Sauvan *et al.* [175]. It used a "cocktail" beam containing a mixture of the nuclides ^{15}B, ^{17}C, $^{19-21}$N, ^{21,23}O, and $^{23-25}$F. One exposure at a fixed setting of the magnetic field of the spectrometer allowed the measurement of the inclusive one-neutron removal cross sections for 22 nuclei at energies ranging from 43–71 MeV/nucleon. The results, representing the sum of the cross sections inside the energy window, are given in Fig. 16. They are compared with theoretical cross sections based on the same approach as in section 4.1 and Fig. 15. The shell-model used the WBP interaction [125]. The reaction calculation was based on [83] and although the S-matrices were constructed in a different way, the end results should be quite similar to those of Fig. 15. The question as to exactly which final states are inside the energy window leads to some systematic uncertainty. Still, the agreement between theory and experiment is very good. The weighted average of the scale factor is $\langle F \rangle = 0.92 \pm 0.04$, where the experimental error has been increased by the square root of the χ^2 per degree of freedom of 3.4.

At the present point in time, the majority of the data favor a scale factor close to unity.

We must, of course, still be prepared to encounter major discrepancies in cases where the fundamental assumptions fail. This can happen if the dominant mechanism is not a direct reaction. The analysis of the ^{11}Be experiment [46] introduced small corrections for the competition from collective excitations caused by Coulomb and nuclear interactions. Two-step interactions must also play a role in certain reactions and small cross sections are, as always, suspect. There are also open experimental questions, especially for more deeply bound states, for which the cross section for diffraction dissociation, see Eq. (4), still needs to be tested esperimentally. Nuclei nearer stability also have more complex spectra, and since the cross sections emerge from an input-output balance of γ-ray intensities, any substantial missed intensity can lead to systematic errors. Fortunately, this problem is smaller near the neutron drip line, where the nuclei have just a few bound levels.

5. CONCLUDING REMARKS

This paper has examined the nature of nuclei near the drip lines. This has been done under three main headings. In section 2 we have considered bound states existing just below the particle threshold, the nuclear halo states. In this area, the qualitative insight that characterized the early work is now being replaced by a more precise understanding. One specific example is Fig. 3, which provides the first "clean" parallel-momentum distribution from nuclear halo dissociation and has stimulated a necessary refinement of the theory. A second example is the study of correlation effects in the two-neutron halo of ^{11}Li, where the superior techniques illustrated in Figs. 5 and 6 offer a more direct handle on the s^2+p^2 mixing. Another precision experiment on ^{12}Be, see section 4.1, now poses the question whether ^{11}Li also could have a very mixed shell structure, involving p^2, s^2 and d^2 components with comparable weights.

Secondly, we have in section 3 considered the energy region just above the particle threshold. Continuum spectroscopy on light nuclei is difficult to perform and to interpret, but it is sometimes necessary. An example of this is the search for the strength of the s–wave coupling in the difficult ^{9}Li+n channel, see section 3.1. This coupling is an essential element in understanding ^{11}Li, see Fig. 9. We also point out that just above a particle threshold one will encounter other continuum features arising from mechanisms that do not have a simple bearing on nuclear structure. They compete with real structural phenomena in a way that it is not always easy to sort out. The whole question of what is a virtual state or a resonance and how one interprets continuum structure is complicated.

The third and maybe most essential part of this paper, section 4, deals with single-nucleon removal reactions at intermediate beam energies. As a spectroscopic tool they show promise of becoming an interesting precision complement to the classical pickup reactions at low energies. Their strength is an extremely high sensitivity, originating in a combination of high reaction probability (thick targets) with inverse kinematics (strong forward focusing). A recent experiment [161] on ^{19}C determined the ground-state mass, j value and spectroscopic factor with an incident ^{19}C beam of less than an atom per second. This technique may develop into one of the main tools in nuclear structure research with radioactive beams in the coming years.

The authors are indebted to B. Alex Brown and Vladimir Zelevinsky for helpful comments.

REFERENCES

1. W. Forsling, C.J. Herrlander and H. Ryde (editors), *Proc. of the International Symp. on Why and How Should We Investigate Nuclides Far Off the Stability Line, Lysekil 1966*, Almqvist and Wiksell (Stockholm 1966) and also as Arkiv for Fysik 36 (1967) pp. 1–686.
2. I. Tanihata (ed.), Research Opportunities with Accelerated Beams of Radioactive Ions, special issue of Nucl. Phys. A.
3. D.A. Bromley (editor), *Treatise on Heavy-Ion Science, Vol. 8: Nuclei Far From Stability*, Plenum (New York, 1989) pp. 1–727.
4. I. Tanihata *in* ref. [3] pp. 443–514.
5. I. Tanihata *et al.*, Phys. Rev. Lett. 55 (1985) 2676; Phys. Lett. B 160 (1985) 380.
6. A. Ozawa, T. Suzuki and I. Tanihata in ref. [2].
7. T. Kobayashi *et al.*, Phys. Rev. Lett. 60 (1988) 2599.
8. P.G. Hansen, A.S. Jensen and B. Jonson. Ann. Rev. Nucl. Part. Sci. 45 (1995) 505.
9. K. Riisager, D. Fedorov and A.S. Jensen, Euro. Phys. Lett. 49 (2000) 547.
10. B. Jonson and K. Riisager, Phil. Trans. R. Soc. Lond. A358 (1998) 2063.
11. R.A. Broglia and P.G. Hansen (editors), *International School of Heavy-Ion Physics, 4^{th} Course: Exotic Nuclei*, (World Scientific, Singapore, 1998) pp. 1–452.
12. C. Rolfs, Nucl. Phys. A 217 (1973) 29.
13. A.M. Mukhamedzhanov and N.K. Timofeyuk, JETP Lett. 51 (1990) 282.
14. H. Esbensen and G.F. Bertsch, Phys. Rev. C 59 (1999) 3240.
15. B.A. Brown and P.G. Hansen, Phys. Lett. B 391 (1996) 391.
16. A. Navin *et al.*, Phys. Rev. Lett. 81 (1998) 5089.
17. I. Tanihata, Prog. Part and Nucl. Phys 35 (1995) 505.
18. B.A. Brown, Phys. Rev. C 58 (1998) 220.
19. J. Dobaczewski and W. Nazarewicz, Phil. Trans. R. Proc. Lond. A356, (1998) 2007.
20. B.A. Brown and W.A. Richter, Phys. Rev. C 54 (1996) 673.
21. B.A. Brown, Phys. Rev. Lett. 85 (2000) 5296.
22. D. Fedorov and A.S. Jensen, Phys. Rev. Lett. 71 (1993) 4103.
23. D. Fedorov, A.S. Jensen and K. Riisager, Phys. Lett. B312 (1993) 1.
24. M.V. Zhukov *et al.*, Phys. Rep. 231 (1993) 151.
25. A.S. Jensen and K. Riisager, Phys. Lett. B 480 (2000) 39.
26. S. Mizutori *et al.*, Phys. Rev. C 61 (2000) 044326.
27. K. Bennaceur *et al.*, Phys. Lett. B 496 (2000) 154.
28. V. Efimov, Phys. Lett. B 33 (1970) 563; Comments Nuc. Part. Phys. 19 (1990) 271.
29. A.E.A. Amorin, T. Frederico and L. Tomio, Phys. Rev. C 56 (1997) R2378.
30. A. Estrin, M. Kotrun, and Y. Hahn, Phys. Rev. C 57 (1998) 50.
31. E. Fermi and E. Teller, Phys. Rev. 72 (1947) 406.
32. C. Desfrancois *et al.*, Europhys. Lett. 26 (1994) 25.
33. P.G. Hansen and B. Jonson, Europhys. Lett. 4 (1987) 409.
34. I. Hamamoto, H. Sagawa, and X.Z. Zhang Phys. Rev. C57 (1998) R1064.
35. E. Garrido, D. Fedorov, and A.S. Jensen, Phys. Lett. B 480 (2000) 32.
36. F. Nunes and I. Thompson, Phys. Rev. C 59 (1999) 2652.
37. V. Guimarães *et al.*, Phys. Rev. Lett. 84 (2000) 1862.

38. D.J. Millener *et al.*, Phys. Rev. C 28 (1983) 497.
39. B. Jonson and K. Riisager, in [2].
40. M.J.G. Borge *et al.*, Phys. Rev. C55 (1997) R8; Nucl. Phys. A 613 (1997) c201.
41. M. Fauerbach *et al*, Phys. Rev. C 56 (1997) R1.
42. M. Fukuda *et al.*, Phys. Lett. B 268 (1991) 339.
43. R. Anne *et al.*, Phys. Lett. B304 (1993) 55-59; Nucl. Phys. A 575,125 (1994).
44. F. Negoita *et al.*, Phys. Rev. C 59 (1999) 2082.
45. K. Hencken, G. Bertsch and H. Esbensen, Phys. Rev. C 54 (1996) 3043.
46. T. Aumann *et al.*, Phys. Rev. Lett. 84 (2000) 35.
47. C.A. Bertulani and G. Baur, Nucl. Phys. A 480 (1988) 615.
48. C.A. Bertulani, L.F. Canto and M.S. Hussein, Physics Reports 81 (1993) pp. 281-378.
49. D.M. Kalassa and G. Baur, J. Phys. G: Nucl. Part. Phys. 22 (1996) 115.
50. H. Esbensen, *in* [11], p. 71.
51. J.A. Tostevin, S. Rugmai and R.C. Johnson, Phys. Rev. C 57 (1998) 3225.
52. Y. Alhassid, M. Gai and G.F. Bertsch, Phys. Rev. Lett. 49 (1982) 1482.
53. H. Esbensen and G.F. Bertsch, Nucl. Phys. A 542 (1992) 310.
54. H. Sagawa, N. Takigawa and N. van Giai, Nucl. Phys. A 543 (1992) 575.
55. P.G. Hansen, Nucl. Phys. A 649 (1999) 355c.
56. T. Nakamura *et al.*, Phys. Lett. B 331 (1994) 296.
57. S. Shimoura *et al.*, Phys. Lett. B 348 (1995) 29.
58. T. Uchiyama and H. Morinaga, Z. Phys. A 320 (1985) 273.
59. A. Mengoni, T. Otsuka, T. Nakamura and M. Ishihara, Nucl. Phys. A 621 (1997) 323c; Phys. Rev. C 52 (1995) R2334.
60. M. Gai *et al.*, Phys. Rev. Lett. 50 (1983) 239.
61. M. Gai *et al.*, Phys. Lett. B 215 (1988) 242.
62. M. Gai *et al.*, Phys. Rev. Lett. 62 (1989) 874.
63. T. Nakamura *et al.*, Phys. Rev. Lett. 83, 1112 (1999).
64. A. Ozawa *et al.*, Measurements of cross sections for light neutron-rich nuclei at relativistic energies and determination of effective matter radii, *RIKEN Report No. RIKEN-AF-NP-376, 2000*, Nucl. Phys. A., in press.
65. G.D. Alkhazov *et al.*, Phys. Rev. Lett., 78 (1998) 2313.
66. C.-B. Moon *et al.*, Phys. Lett. B 297 (1992) 39.
67. A.A. Korsheninnikov *et al.* Phys. Rev. Lett. 78 (1997) 2317.
68. S. Karataglidis *et al.*, Phys. Rev. Lett. 79 (1997) 1447; Phys. Rev. C 61 (2000) 024319.
69. E.F. Aguilera *et al.*, Phys. Rev. Lett. 84 (2000) 5058.
70. J.J. Kolata *et al.*, Phys. Rev. Lett. 81 (1998) 4580.
71. M. Trotta *et al.*, Phys. Rev. Lett. 84 (2000) 2342.
72. A. Yoshida *et al.*, Phys. Lett. B 389 (1996) 457.
73. V. Fekou-Youmbi *et al.*, Nucl. Instr. Meth. A 437 (1999) 490.
74. K.E. Rehm *et al.*, Phys. Rev. Lett. 81 (1998) 3341.
75. F. Barranco and E. Vigezzi, *in* [11], p. 217.
76. B. Jonson, *in* [11] p.93.
77. G.F. Bertsch, B.A. Brown and H. Sagawa, Phys. Rev. C 39 (1989) 1154.
78. G.F. Bertsch, H. Esbensen, and A. Sustich, Phys. Rev. C 42 (1990) 758.
79. K. Yabana, Y. Ogawa, and Y. Suzuki, Nucl. Phys. A 539 (1992) 293.

80. P.G. Hansen, in *Proceedings of the Int. Conf. on Exotic Nuclei and Atomic Masses, Arles, France, June 1995*, edited by M. de Saint Simon and O. Sorlin (Editions Frontières, Orsay, 1995), pp. 175-186.
81. P.G. Hansen, Phys. Rev. Lett. 77 (1996) 1016.
82. H. Esbensen, Phys. Rev. C 53 (1996) 2007.
83. J.A. Tostevin, J. Phys. G 25 (1999) 735.
84. M.S. Hussein and K.W. McVoy, Nucl. Phys. A 445 (1985) 124.
85. J.S. Al-Khalili, J.A. Tostevin, and I.J. Thompson, Phys. Rev. C 54 (1996) 1843.
86. J.A. Tostevin and J.S. Al-Khalili, Nucl. Phys. A 616 (1997) 418c.
87. R.J. Glauber, in *Lectures in Theoretical Physics*, edited by W.E. Brittin (Interscience, New York, 1959), Vol. 1, p. 315.
88. S. Kox *et al.*, Phys. Rev. C 35 (1987) 1678.
89. J.H. Kelley *et al.*, Phys. Rev. Lett. 74 (1995) 30.
90. J. Tostevin, Nucl. Phys. A 682 (2001) 320c.
91. A. Bonaccorso and D.M. Brink, Phys. Rev. C 57 (1998) R22.
92. A. Bonaccorso and D.M. Brink, Phys. Rev. C 58 (1998) 2864.
93. A. Bonaccorso, Phys. Rev. C 60 (1999) 054604.
94. R. Anne *et al.*, Phys. Lett. B 250 (1990) 19.
95. F. Barranco and P.G. Hansen, Eur. Phys. J. A. 7 (2000) 179.
96. J.Margueron, A. Bonaccorso and D.M. Brink, Coulomb-nuclear interference ffects in the breakup of halo nuclei, to be published (2001).
97. M. Fallot *et al.*, Coulomb versus nuclear breakup of ^{11}Be halo nucleus in a non-perturbative framework, IPNO DR 00-35 and to be published.
98. J.A. Scarpaci *et al.*, Phys. Lett. B 428 (1998) 241.
99. R.E. Warner *et al.*, Phys. Rev. C 52 (1995) R1166.
100. M.H. Smedberg *et al.*, Phys. Lett. B 452 (1999) 1.
101. J.H. Kelley *et al.*, Phys. Rev. Lett. 77 (1996) 5020.
102. E. Garrido, D.V. Fedorov and A.S. Jensen, Europhys. Lett. 50 (2000) 735; Phys. Rev. C 59 (1999) 1272; Phys. Rev. C 55 (1997) 1327; Phys. Rev. C 53 (1996) 3159.
103. E. Garrido, D.V. Fedorov and A.S. Jensen, Phys. Rev. C 58 (1998) R2654.
104. A. Cobis, D.V. Fedorov and A.S. Jensen Phys. Rev. C 58 (1998) 1403.
105. D.J. Morrissey *et al.*, Nucl. Phys. A. 627 (1997) 222.
106. N. Aoi *et al.*, Z. Phys. A 358 (1997) 253.
107. F. Barranco, E. Vigezzi and R.A. Broglia, Phys. Lett. B 319 (1993) 387.
108. H. Simon *et al.*, Phys. Rev. Lett. 83 (1999) 496.
109. J.C. Slater, *The Quantum Theory of Matter* (McGraw-Hill 1968) p. 442.
110. K. Markenroth *et al.*, Nucl. Phys. A 679 (2001) 462.
111. P.J. Woods and C.N. Davids, Ann. Rev. Nucl. Part. Sci. 47 (1997) 541.
112. C.N. Davids *et al.*, Phys. Rev. Lett. 80 (1998) 1849.
113. K. Bennaceur *et al.*, Nucl. Phys. A 651 (1999) 289.
114. B.M. Young *et al.*, Phys. Rev. C49 (1994) 279.
115. J.A. Caggiano *et al.*, Phys. Rev. C60 (1999) 064322.
116. M. Thoennessen *et al.*, Phys. Rev. C59 (1999) 111.
117. L. Chen, B. Blank, B.A. Brown, M. Chartier, A. Galonsky, P.G. Hansen and M. Thoennessen, Phys. Lett. B 505 (2001) 21.

118.K.K. Seth *et al.*, Phys. Rev. Lett. 58, 1930 (1987).
119.H.G. Bohlen *et al.*, Z. Phys. A 330, 227 (1988).
120.W. von Oertzen *et al.*, Nucl. Phys. A588, 129c (1995).
121.A.A. Ogloblin, Z. Phys. A 351, 355 (1995).
122.R.A. Kryger *et al.*, Phys. Rev. C 37, R2439 (1993).
123.L.D. Landau and E.M. Lifshitz, *Quantum Mechanics (Non-relativistic Theory)* (Pergamon Press, Oxford, 1977) pp. 552-557.
124.B.A. Brown, B.H. Wildenthal, Ann. Rev. Nucl. Part. Sci. 38 (1988) 29.
125.E.K. Warburton and B.A. Brown, Phys. Rev. C **46**, 923 (1992).
126.M. Zinser *et al.*, Phys. Rev. Lett. 75, 1719 (1995).
127.M. Zinser *et al.*, Nucl. Phys. A619, 151 (1997).
128.G.F. Bertsch, K. Hencken and H. Esbensen, *et al.*, Phys. Rev. C 57, 1366 (1998).
129.P.G. Hansen, Nucl. Phys. A 682 (2001) 310c.
130.A. Azhari *et al.*, Phys. Rev. C 57 (1998) 628.
131.J.M. Oliveira *et al.*, Phys. Rev. Lett. 84 (2000) 4056.
132.K. Markenroth *et al.*, Phys. Rev. C 62 (2000) 034308.
133.R. Sherr, private communication cited in Ref. [132].
134.F.C. Barker and P.B. Treacy, Nucl. Phys. 38 (1962) 33.
135.F.C. Barker, G.M. Crawley, P.S. Miller and W.F. Steele, Aust. J. Phys. 29 (1976) 245.
136.B. Crasemann (ed.), in *Atomic Inner-Shell Physics*, published in the series physics of Atoms and Molecules (Plenum, 1985), pp. 1-754.
137.M.S. Freedman, Ann. Rev. Nucl. Sci. 24 (1974) 209.
138.J. Lindhard and P.G. Hansen, Phys. Rev. Lett. 57 (1986) 965.
139.A. Navin *et al.*, Phys. Rev. Lett. 85 (2000) 266.
140.H.J. Lipkin, *Quantum Mechanics* (North-Holland, Amsterdam 1988) pp. 30-110.
141.A. Pushkin, B. Jonson and M.V. Zhukov, J. Phys. G 22 (1996) L95.
142.R.C. Johnson, J.S. Al-Khalili and J.A. Tostevin, Phys. Rev. Lett. 79 (1997) 266.
143.D. Aleksandrov *et al.*, Nucl.Phys. A 669 (2000) 51.
144.S. Nakayama *et al.*, Phys. Rev. Lett. 85 (2000) 262.
145.C. Forssen, B. Jonson and M.V. Zhukov, Nucl. Phys. A 673 (2000) 143.
146.B.V. Danilin, I.J. Thompson, J.S. Vaagen and M.V. Zhukov, Nucl.Phys. A 632 (1998) 383.
147.P. Navratil and B.R. Barrett Phys. Rev. C 57 (1998) 3119.
148.R.B. Wiringa, S.C. Pieper, J. Carlson and V.R. Pandharipande Phys. Rev. C 62 (2000) 0114001.
149.A.A. Korsheninnikov *et al.*, Phys. Lett. B 326 (1994) 31.
150.A.N. Ostrowski *et al.*, Phys. Lett. B 338 (1994) 13.
151.T. Kobayashi *et al.*, Nucl.Phys. A 616 (1997) 223c.
152.G. Audi, O. Bersillon, J. Blachot and A.H. Wapstra, Nucl.Phys. A 624 (1997) 1.
153.Aa. Bohr and B.R. Mottelson, *Nuclear Structure* (Benjamin, New York, 1969 and 1975), Vol. 1, p. 420 and Vol. 2, p. 243, 258.
154.G.R. Satchler, *Direct Nuclear reactions* (University Press, Oxford, 1983) pp. 1-833.
155.H. Feshbach, *Theoretical Nuclear Physics: Nuclear Reactions* (Wiley, New York, 1992), p. 455.
156.S. Fortier *et al.*, Phys. Lett. B 461 (1999) 461.

157. J.S. Winfield *et al.*, Nucl. Phys. A 683 (2001) 48.
158. K.E. Rehm *et al.*, Phys. Rev. Lett. 80 (1998) 676; Nucl. Instr. Meth. A 449 (2000) 208.
159. A.A. Korsheninnikov *et al.*, Phys. Rev. Lett. 82 (1999) 3581.
160. V. Guimarães *et al.*, Phys. Rev. C 61 (2000) 064609.
161. V. Maddalena *et al.*, Phys. Rev. C. 63 (2001) 024613.
162. J.A. Tostevin *et al.*, to be published.
163. R. Serber, Phys. Rev. 72 (1947) 1008; Annu. Rev. Nucl. Part. Sci. 44 (1994) 1.
164. P. Kitching, W.J. McDonald, Th.A. Maris and C.A.Z. Vasconcellos, Adv. Nucl. Phys. 15 (1985) 43.
165. H. Sagawa and K. Yazaki, Phys. Lett. B 244 (1990) 149.
166. P.G. Hansen, J. Phys. G 25 (1999) 727.
167. B.A. Brown, *in* [11] p. 1.
168. J. Dobaczewski *et al.*, Phys. Rev. Lett. 72 (1994) 981.
169. F.C. Barker, J. Phys. G 2 (1976) L45; Phys. Rev. C 59 (1999) 535.
170. R. Sherr and H.T. Fortune, Phys. Rev. C 60 (1999) 064323.
171. H. Iwazaki *et al.*, Phys. Lett. B 481 (2000) 7; Phys. Lett. B 491 (2000) 8.
172. D.R. Tilley, H.R. Weller, and C.M. Cheves, Nucl. Phys. A **564**, 1 (1993).
173. A. Sakharuk and V. Zelevinsky, Phys. Rev. C 61 (1999) 014609.
174. J.A. Tostevin, in *Fission and Properties of Neutron-rich Nuclei*, Proceedings of the Second International Conference, St Andrews, Scotland, 28 June - 3 July 1999, edited by J.H. Hamilton, W.R. Phillips, and H.K. Carter (World Scientific, Singapore, March 2000), p. 429.
175. E. Sauvan *et al.*, Phys. Lett. B 491 (2000) 1.